

# Measurement of the $e^+e^- \rightarrow W^+W^-$ cross section and $W$ decay branching fractions at LEP

*This paper is dedicated to the memory of Ben Shen.*

The OPAL Collaboration

G. Abbiendi<sup>2</sup>, C. Ainsley<sup>5</sup>, P.F. Åkesson<sup>7</sup>, G. Alexander<sup>21</sup>, G. Anagnostou<sup>1</sup>, K.J. Anderson<sup>8</sup>, S. Asai<sup>22,23</sup>, D. Axen<sup>27</sup>, I. Bailey<sup>26</sup>, E. Barberio<sup>7,49</sup>, T. Barillari<sup>32</sup>, R.J. Barlow<sup>15</sup>, R.J. Batley<sup>5</sup>, P. Bechtel<sup>25</sup>, T. Behnke<sup>25</sup>, K.W. Bell<sup>19</sup>, P.J. Bell<sup>1</sup>, G. Bella<sup>21</sup>, A. Bellerive<sup>6</sup>, G. Benelli<sup>4</sup>, S. Bethke<sup>32</sup>, O. Biebel<sup>31</sup>, O. Boeriu<sup>9</sup>, P. Bock<sup>10</sup>, M. Boutemeur<sup>31</sup>, S. Braibant<sup>2</sup>, R.M. Brown<sup>19</sup>, H.J. Burckhart<sup>7</sup>, S. Campana<sup>4</sup>, P. Capiluppi<sup>2</sup>, R.K. Carnegie<sup>6</sup>, A.A. Carter<sup>12</sup>, J.R. Carter<sup>5</sup>, C.Y. Chang<sup>16</sup>, D.G. Charlton<sup>1</sup>, C. Ciocca<sup>2</sup>, A. Csilling<sup>29</sup>, M. Cuffiani<sup>2</sup>, S. Dado<sup>20</sup>, M. Dallavalle<sup>2</sup>, A. De Roeck<sup>7</sup>, E.A. De Wolf<sup>7,50</sup>, K. Desch<sup>25</sup>, B. Dienes<sup>30</sup>, J. Dubbert<sup>31</sup>, E. Duchovni<sup>24</sup>, G. Duckeck<sup>31</sup>, I.P. Duerdoth<sup>15</sup>, E. Etzion<sup>21</sup>, F. Fabbri<sup>2</sup>, P. Ferrari<sup>7</sup>, F. Fiedler<sup>31</sup>, I. Fleck<sup>9</sup>, M. Ford<sup>15</sup>, A. Frey<sup>7</sup>, P. Gagnon<sup>11</sup>, J.W. Gary<sup>4</sup>, C. Geich-Gimbel<sup>3</sup>, G. Giacomelli<sup>2</sup>, P. Giacomelli<sup>2</sup>, M. Giunta<sup>4</sup>, J. Goldberg<sup>20</sup>, E. Gross<sup>24</sup>, J. Grunhaus<sup>21</sup>, M. Gruwé<sup>7</sup>, A. Gupta<sup>8</sup>, C. Hajdu<sup>29</sup>, M. Hamann<sup>25</sup>, G.G. Hanson<sup>4</sup>, A. Harel<sup>20</sup>, M. Hauschild<sup>7</sup>, C.M. Hawkes<sup>1</sup>, R. Hawkings<sup>7</sup>, G. Herten<sup>9</sup>, R.D. Heuer<sup>25</sup>, J.C. Hill<sup>5</sup>, D. Horváth<sup>29,36</sup>, P. Igo-Kemenes<sup>10</sup>, K. Ishii<sup>22,23</sup>, H. Jeremie<sup>17</sup>, P. Jovanovic<sup>1</sup>, T.R. Junk<sup>6,42</sup>, J. Kanzaki<sup>22,23,54</sup>, D. Karlen<sup>26</sup>, K. Kawagoe<sup>22,23</sup>, T. Kawamoto<sup>22,23</sup>, R.K. Keeler<sup>26</sup>, R.G. Kellogg<sup>16</sup>, B.W. Kennedy<sup>19</sup>, S. Kluth<sup>32</sup>, T. Kobayashi<sup>22,23</sup>, M. Kobel<sup>3,53</sup>, S. Komamiya<sup>22,23</sup>, T. Krämer<sup>25</sup>, A. Krasznahorkay Jr.<sup>30,38</sup>, P. Krieger<sup>6,45</sup>, J. von Krogh<sup>10</sup>, T. Kuhl<sup>25</sup>, M. Kupper<sup>24</sup>, G.D. Lafferty<sup>15</sup>, H. Landsman<sup>20</sup>, D. Lanske<sup>13</sup>, D. Lellouch<sup>24</sup>, J. Letts<sup>48</sup>, L. Levinson<sup>24</sup>, J. Lillich<sup>9</sup>, S.L. Lloyd<sup>12</sup>, F.K. Loebinger<sup>15</sup>, J. Lu<sup>27,35</sup>, A. Ludwig<sup>3,53</sup>, J. Ludwig<sup>9</sup>, W. Mader<sup>3,53</sup>, S. Marcellini<sup>2</sup>, A.J. Martin<sup>12</sup>, T. Mashimo<sup>22,23</sup>, P. Mättig<sup>46</sup>, J. McKenna<sup>27</sup>, R.A. McPherson<sup>26</sup>, F. Meijers<sup>7</sup>, W. Menges<sup>25</sup>, F.S. Merritt<sup>8</sup>, H. Mes<sup>6,34</sup>, N. Meyer<sup>25</sup>, A. Michelini<sup>2</sup>, S. Mihara<sup>22,23</sup>, G. Mikenberg<sup>24</sup>, D.J. Miller<sup>14</sup>, W. Mohr<sup>9</sup>, T. Mori<sup>22,23</sup>, A. Mutter<sup>9</sup>, K. Nagai<sup>12</sup>, I. Nakamura<sup>22,23,55</sup>, H. Nanjo<sup>22,23</sup>, H.A. Neal<sup>33</sup>, S.W. O’Neale<sup>1,a</sup>, A. Oh<sup>7</sup>, M.J. Oreglia<sup>8</sup>, S. Orito<sup>22,23,a</sup>, C. Pahl<sup>32</sup>, G. Pásztor<sup>4,40</sup>, J.R. Pater<sup>15</sup>, J.E. Pilcher<sup>8</sup>, J. Pinfold<sup>28</sup>, D.E. Plane<sup>7,b</sup>, O. Pooth<sup>13</sup>, M. Przybycień<sup>7,47</sup>, A. Quadt<sup>32</sup>, K. Rabbertz<sup>7,50</sup>, C. Rember<sup>7</sup>, P. Renkel<sup>24</sup>, J.M. Roney<sup>26</sup>, A.M. Rossi<sup>2</sup>, Y. Rozen<sup>20</sup>, K. Runge<sup>9</sup>, K. Sachs<sup>6</sup>, T. Saeki<sup>22,23</sup>, E.K.G. Sarkisyan<sup>7,43</sup>, A.D. Schaile<sup>31</sup>, O. Schaile<sup>31</sup>, P. Scharff-Hansen<sup>7</sup>, J. Schieck<sup>32</sup>, T. Schörner-Sadenius<sup>7,58</sup>, M. Schröder<sup>7</sup>, M. Schumacher<sup>3</sup>, R. Seuster<sup>13,39</sup>, T.G. Shears<sup>7,41</sup>, B.C. Shen<sup>4,a</sup>, P. Sherwood<sup>14</sup>, A. Skuja<sup>16</sup>, A.M. Smith<sup>7</sup>, R. Sobie<sup>26</sup>, S. Söldner-Rembold<sup>15</sup>, F. Spano<sup>8,57</sup>, A. Stahl<sup>13</sup>, D. Strom<sup>18</sup>, R. Ströhmer<sup>31</sup>, S. Tarem<sup>20</sup>, M. Tasevsky<sup>7,37</sup>, R. Teuscher<sup>8</sup>, M.A. Thomson<sup>5</sup>, E. Torrence<sup>18</sup>, D. Toya<sup>22,23</sup>, I. Trigger<sup>7,56</sup>, Z. Trócsányi<sup>30,38</sup>, E. Tsur<sup>21</sup>, M.F. Turner-Watson<sup>1</sup>, I. Ueda<sup>22,23</sup>, B. Ujvári<sup>30,38</sup>, C.F. Vollmer<sup>31</sup>, P. Vannerem<sup>9</sup>, R. Vértési<sup>30,38</sup>, M. Verzocchi<sup>16</sup>, H. Voss<sup>7,50</sup>, J. Vossebeld<sup>7,41</sup>, C.P. Ward<sup>5</sup>, D.R. Ward<sup>5</sup>, P.M. Watkins<sup>1</sup>, A.T. Watson<sup>1</sup>, N.K. Watson<sup>1</sup>, P.S. Wells<sup>7</sup>, T. Wengler<sup>7</sup>, N. Wermes<sup>3</sup>, G.W. Wilson<sup>15,44</sup>, J.A. Wilson<sup>1</sup>, G. Wolf<sup>24</sup>, T.R. Wyatt<sup>15</sup>, S. Yamashita<sup>22,23</sup>, D. Zer-Zion<sup>4</sup>, L. Zivkovic<sup>20</sup>

<sup>1</sup> School of Physics and Astronomy, University of Birmingham, Birmingham B15 2TT, UK

<sup>2</sup> Dipartimento di Fisica dell’Università di Bologna and INFN, 40126 Bologna, Italy

<sup>3</sup> Physikalisches Institut, Universität Bonn, 53115 Bonn, Germany

<sup>4</sup> Department of Physics, University of California, Riverside CA 92521, USA

<sup>5</sup> Cavendish Laboratory, Cambridge CB3 0HE, UK

<sup>6</sup> Ottawa-Carleton Institute for Physics, Department of Physics, Carleton University, Ottawa, Ontario K1S 5B6, Canada

<sup>7</sup> CERN, European Organisation for Nuclear Research, 1211 Geneva 23, Switzerland

<sup>8</sup> Enrico Fermi Institute and Department of Physics, University of Chicago, Chicago IL 60637, USA

<sup>9</sup> Fakultät für Physik, Albert-Ludwigs-Universität Freiburg, 79104 Freiburg, Germany

<sup>10</sup> Physikalisches Institut, Universität Heidelberg, 69120 Heidelberg, Germany

<sup>11</sup> Indiana University, Department of Physics, Bloomington IN 47405, USA

<sup>12</sup> Queen Mary and Westfield College, University of London, London E1 4NS, UK

<sup>13</sup> Technische Hochschule Aachen, III Physikalisches Institut, Sommerfeldstrasse 26–28, 52056 Aachen, Germany

<sup>14</sup> University College London, London WC1E 6BT, UK

<sup>15</sup> School of Physics and Astronomy, Schuster Laboratory, The University of Manchester M13 9PL, UK

<sup>16</sup> Department of Physics, University of Maryland, College Park, MD 20742, USA

<sup>17</sup> Laboratoire de Physique Nucléaire, Université de Montréal, Montréal, Québec H3C 3J7, Canada

<sup>18</sup> University of Oregon, Department of Physics, Eugene OR 97403, USA

<sup>19</sup> Rutherford Appleton Laboratory, Chilton, Didcot, Oxfordshire OX11 0QX, UK

- 20 Department of Physics, Technion-Israel Institute of Technology, Haifa 32000, Israel  
 21 Department of Physics and Astronomy, Tel Aviv University, Tel Aviv 69978, Israel  
 22 International Centre for Elementary Particle Physics and Department of Physics, University of Tokyo, Tokyo 113-0033, Japan  
 23 Kobe University, Kobe 657-8501, Japan  
 24 Particle Physics Department, Weizmann Institute of Science, Rehovot 76100, Israel  
 25 Universität Hamburg/DESY, Institut für Experimentalphysik, Notkestrasse 85, 22607 Hamburg, Germany  
 26 University of Victoria, Department of Physics, P.O. Box 3055, Victoria BC V8W 3P6, Canada  
 27 University of British Columbia, Department of Physics, Vancouver BC V6T 1Z1, Canada  
 28 University of Alberta, Department of Physics, Edmonton AB T6G 2J1, Canada  
 29 Research Institute for Particle and Nuclear Physics, 1525 Budapest, P.O. Box 49, Hungary  
 30 Institute of Nuclear Research, 4001 Debrecen, P.O. Box 51, Hungary  
 31 Ludwig-Maximilians-Universität München, Sektion Physik, Am Coulombwall 1, 85748 Garching, Germany  
 32 Max-Planck-Institute für Physik, Föhringer Ring 6, 80805 München, Germany  
 33 Yale University, Department of Physics, New Haven, CT 06520, USA  
 34 and at TRIUMF, Vancouver, Canada V6T 2A3  
 35 now at University of Alberta  
 36 and Institute of Nuclear Research, Debrecen, Hungary  
 37 now at Institute of Physics, Academy of Sciences of the Czech Republic 18221 Prague, Czech Republic  
 38 and Department of Experimental Physics, University of Debrecen, Hungary  
 39 and MPI München  
 40 and Research Institute for Particle and Nuclear Physics, Budapest, Hungary  
 41 now at University of Liverpool, Dept of Physics, Liverpool L69 3BX, UK  
 42 now at Dept. Physics, University of Illinois at Urbana-Champaign, USA  
 43 and University of Antwerpen, 2610 Antwerpen, Belgium  
 44 now at University of Kansas, Dept of Physics and Astronomy, Lawrence, KS 66045, USA  
 45 now at University of Toronto, Dept of Physics, Toronto, Canada  
 46 current address Bergische Universität, Wuppertal, Germany  
 47 now at University of Mining and Metallurgy, Cracow, Poland  
 48 now at University of California, San Diego, USA  
 49 now at The University of Melbourne, Victoria, Australia  
 50 now at IPHE Université de Lausanne, 1015 Lausanne, Switzerland  
 51 now at IEKP Universität Karlsruhe, Germany  
 52 now at University of Antwerpen, Physics Department, 2610 Antwerpen, Belgium<sup>c</sup>  
 53 now at Technische Universität, Dresden, Germany  
 54 and High Energy Accelerator Research Organisation (KEK), Tsukuba, Ibaraki, Japan  
 55 now at University of Pennsylvania, Philadelphia, Pennsylvania, USA  
 56 now at TRIUMF, Vancouver, Canada  
 57 now at Columbia University  
 58 now at DESY

Received: 22 July 2007 / Revised version: 10 September 2007 /

Published online: 19 October 2007 – © Springer-Verlag / Società Italiana di Fisica 2007

**Abstract.** From a total data sample of  $701.1 \text{ pb}^{-1}$  recorded with  $e^+e^-$  centre-of-mass energies of  $\sqrt{s} = 161\text{--}209 \text{ GeV}$  with the OPAL detector at LEP, 11693  $W$ -pair candidate events are selected. These data are used to obtain measurements of the  $W$ -pair production cross sections at 10 different centre-of-mass energies. The ratio of the measured cross sections to the standard model expectation is found to be:

$$\text{data/SM} = 1.002 \pm 0.011(\text{stat.}) \pm 0.007(\text{syst.}) \pm 0.005(\text{theory}),$$

where the uncertainties are statistical, experimental systematics and theory systematics respectively. The data are used to determine the  $W$  boson branching fractions, which are found to be consistent with lepton universality of the charged current interaction. Assuming lepton universality, the branching ratio to hadrons is determined to be  $67.41 \pm 0.37(\text{stat.}) \pm 0.23(\text{syst.})\%$ , from which the CKM matrix element  $|V_{cs}|$  is determined to be  $0.969 \pm 0.017(\text{stat.}) \pm 0.012(\text{syst.})$ . The differential cross section as a function of the  $W^-$  production angle is measured for the  $qqe\nu$  and  $qq\nu\nu$  final states. The results described in this paper are consistent with the expectations from the standard model.

<sup>a</sup> Deceased

<sup>b</sup> e-mail: David.Plane@cern.ch

<sup>c</sup> supported by Interuniversity Attraction Poles Programme – Belgian Science Policy

## 1 Introduction

From 1996 to 2000 the LEP  $e^+e^-$  collider at CERN operated at centre-of-mass energies,  $\sqrt{s}$ , above the threshold

for  $W^+W^-$  production. This paper describes the OPAL measurements of the  $W^+W^-$  production cross section and  $W$  branching fractions using this data sample that corresponds to a total integrated luminosity of  $701.1 \text{ pb}^{-1}$ . The OPAL analysis of  $W^+W^-$  production and decay using data recorded at  $\sqrt{s} > 190 \text{ GeV}$  has not been published previously. For this paper the data recorded at  $183 \text{ GeV}$  and above have been analysed using the final OPAL detector calibration and  $W$  pair event selections. The results presented here supersede the previous OPAL analysis of the data recorded at  $\sqrt{s} = 183 \text{ GeV}$  [1] and  $\sqrt{s} = 189 \text{ GeV}$  [2]. The data collected close to the  $W$  pair production threshold ( $\sqrt{s} = 161 \text{ GeV}$  and  $172 \text{ GeV}$ ) have not been reanalysed and the corresponding results are described in [3, 4]. Furthermore, for the reasons explained in Sect. 3.1, the  $183 \text{ GeV } W^+W^- \rightarrow \ell\nu\ell\nu$  data have not been reanalysed and the corresponding results are given in [1].

In this paper,  $W^+W^-$  production is defined in terms of the CC03 class [5] of production diagrams. These diagrams, which correspond to  $t$ -channel  $\nu_e$  exchange and  $s$ -channel  $Z/\gamma$  exchange, provide a natural definition of resonant  $W$ -pair production. The contributions to the event rate from non-CC03 diagrams which lead to the same final states as  $W$ -pair production (including interference with the CC03 set of diagrams) are treated as additive background. In the standard model (SM),  $W^+W^-$  events are expected to decay into fully leptonic ( $\ell\nu\ell\nu$ ), semi-leptonic ( $q\ell\nu$ ), or fully hadronic ( $qqqq$ ) final states with predicted SM branching fractions of 10.6%, 43.9% and 45.6% respectively [5]. Here  $qq$  denotes a quark and an anti-quark and  $\ell\nu$  denotes a lepton/anti-lepton ( $\ell = e, \mu, \tau$ ) and an anti-neutrino/neutrino. Three separate event selections, described in Sect. 3, are used to identify candidate  $W^+W^-$  events by their final state topologies with  $\ell\nu\ell\nu$  and  $q\ell\nu$  candidates classified according to the charged lepton type. From the observed event rates in these ten channels (6  $\ell\nu\ell\nu$ , 3  $q\ell\nu$  and  $qqqq$ ) measurements of the  $W$  boson branching fractions and total  $W^+W^-$  production cross section are obtained. The measured branching fraction to hadrons is used to provide a determination of the CKM matrix element  $|V_{cs}|$ . For the  $qqe\nu_e$  and  $qq\mu\nu_\mu$  decay channels the charge of the  $W$  bosons can be identified from the charge of the observed lepton. These events are used to determine the differential cross section in terms of the  $W^-$  polar angle.

## 2 Detector, data and Monte Carlo samples

### 2.1 The OPAL detector

The inner part of the Opal detector consisted of a 3.7 m diameter tracking volume within a 0.435 T axial magnetic field. The tracking detectors included a silicon micro-vertex detector, a high precision gas vertex detector and a large volume gas jet chamber. The tracking acceptance corresponds to approximately  $|\cos\theta| < 0.95$  (for the track quality cuts used in this study), where  $\theta$  is the polar angle with respect to the  $e^-$  beam direction. The trans-

verse momentum resolution for muon tracks is approximately  $\sigma_{p_T}/p_T = \sqrt{(0.02)^2 + (0.0015p_T)^2}$  with  $p_T$  measured in GeV. Lying outside the solenoid, the electromagnetic calorimeter (ECAL) consisting of 11 704 lead glass blocks had full acceptance in the range  $|\cos\theta| < 0.98$  and a relative energy resolution for electrons of approximately  $\sigma_E/E \approx 0.18/\sqrt{E}$  with  $E$  measured in GeV. The magnet return yoke was instrumented with streamer tubes which served as the hadronic calorimeter. Muon chambers outside the hadronic calorimeter provided muon identification in the range  $|\cos\theta| < 0.98$ . Hermeticity for polar angles down to approximately 24 mrad was achieved with forward detectors designed for measuring electrons and photons. Additional forward scintillator tiles were installed in 1998 in order to extend the coverage for detection of minimum ionising particles [6]. These forward scintillator tiles were used to improve the  $\ell\nu\ell\nu$  analysis for the  $\sqrt{s} \geq 189 \text{ GeV}$  data samples. A detailed description of the Opal detector can be found in [7–9].

### 2.2 Data sample

From 1996 onwards the centre-of-mass energy of the LEP collider was increased from 161 GeV to 209 GeV in several steps. The total integrated luminosity of the data sample considered in this paper, evaluated using small angle Bhabha scattering events observed in the silicon tungsten forward calorimeter [10], is  $701.1 \pm 2.1 \text{ pb}^{-1}$ . For the purpose of measuring the  $W^+W^-$  cross section these data are divided into ten  $\sqrt{s}$  ranges listed in Table 1. These ranges reflect the main energy steps as the centre-of-mass energy was increased during LEP operation above the  $W^+W^-$  production threshold.

### 2.3 Monte Carlo samples

A number of Monte Carlo (MC) samples, all including a full simulation[11] of the Opal detector, are used to

**Table 1.** The energy binning used for the  $W^+W^-$  cross section measurements. The  $\sqrt{s}$  range covered by each bin, the mean luminosity-weighted value of  $\sqrt{s}$  and the corresponding integrated luminosity,  $\mathcal{L}$ , are listed

Range/GeV	$\langle\sqrt{s}\rangle/\text{GeV}$	$\mathcal{L}/\text{pb}^{-1}$
160.0–165.0	161.30	9.89
165.0–180.0	172.11	10.36
180.0–185.0	182.68	57.38
185.0–190.0	188.63	183.04
190.0–194.0	191.61	29.33
194.0–198.0	195.54	76.41
198.0–201.0	199.54	76.58
201.0–202.5	201.65	37.68
202.5–205.5	204.88	81.91
205.5–209.0	206.56	138.54
Total	–	701.12

model the signal and background processes. For this paper the main MC samples for four-fermion final states consistent with coming from the process  $e^+e^- \rightarrow W^+W^-$  are generated using the KandY [12] program. KandY includes exact  $\mathcal{O}(\alpha)$  YFS exponentiation [13] for the  $W^+W^-$  production process, with  $\mathcal{O}(\alpha)$  electroweak non-leading (NL) corrections combined with YFS exponentiated  $\mathcal{O}(\alpha^3)$  leading logarithm (LL) initial state radiation (ISR). Final state radiation (FSR) from leptons is implemented in Photos [14] and radiation from the quark induced parton-shower is performed by Jetset [15, 16]. The hadronisation within the Jetset model is tuned to Opal data recorded at the  $Z$  resonance [17]. For the studies of systematic uncertainties the Jetset hadronisation model is compared with the predictions from Herwig [18, 19] and Ariadne [20].

The KandY generator is also used to produce event weights such that generated events can be reweighted to correspond to the CC03 set of diagrams alone. The difference between the full set of four-fermion diagrams and the CC03 diagrams alone is used to obtain the four-fermion background which includes the effects of interference with the CC03 diagrams.

The KoralW program [21–23] is used to simulate the background from four-fermion final states which are incompatible with coming from the decays of two  $W$ -bosons (e.g.  $e^+e^- \rightarrow qq\mu^+\mu^-$ ). The two-fermion background processes  $e^+e^- \rightarrow Z/\gamma \rightarrow \mu^+\mu^-$ ,  $e^+e^- \rightarrow Z/\gamma \rightarrow \tau^+\tau^-$  and  $e^+e^- \rightarrow Z/\gamma \rightarrow qq$  are simulated using KK2f [24, 25]. The two fermion process  $e^+e^- \rightarrow Z/\gamma \rightarrow e^+e^-$  is simulated using Bhwide [26]. Backgrounds from two-photon interactions are evaluated using Pythia [27], Herwig, Phojet [28, 29], BDK [30, 31] and the Vermaseren program [32].

The SM predictions for the CC03  $e^+e^- \rightarrow W^+W^-$  cross sections above the  $W^+W^-$  threshold region are obtained from the YfsWW [33, 34] and the RacoonWW [35, 36] programs. RacoonWW is a complete  $\mathcal{O}(\alpha)$   $e^+e^- \rightarrow 4f\gamma$  calculation in the double pole approximation with ISR treated using a structure function approach. The

YfsWW program provides the  $W^+W^-$  calculations in KandY. YfsWW and RacoonWW yield nearly identical predictions for the  $W^+W^-$  cross sections with an estimated theoretical uncertainty of approximately 0.5% [37]. For  $W$ -pair production near threshold (the 161 GeV and 172 GeV data) the leading- and double-pole approximations used in YfsWW and RacoonWW respectively are no longer valid and the predictions are obtained using the improved Born approximation with a theoretical uncertainty of approximately 2%.

### 3 $e^+e^- \rightarrow W^+W^-$ event selection

The selection of  $W^+W^-$  events proceeds in three stages, corresponding to the three  $W^+W^-$  decay topologies:  $W^+W^- \rightarrow \ell\nu\ell\nu$ ,  $W^+W^- \rightarrow qql\nu$  and  $W^+W^- \rightarrow qqqq$ . The selections are mutually exclusive with only events failing the  $W^+W^- \rightarrow \ell\nu\ell\nu$  selection being considered in the  $W^+W^- \rightarrow qql\nu$  selection, and only events which are not selected as  $\ell\nu\ell\nu$  or  $qql\nu$  being considered for the  $W^+W^- \rightarrow qqqq$  selection. The event selections are essentially unchanged from those described in detail in [2] (and references therein) although the  $W^+W^- \rightarrow \ell\nu\ell\nu$  selection now incorporates features used in the Opal analysis of di-lepton events with significant missing transverse momentum [38].

In the centre-of-mass energy range  $\sqrt{s} = 161\text{--}209$  GeV, the luminosity-weighted average CC03  $W$ -pair selection efficiencies for the  $\ell\nu\ell\nu$ ,  $qql\nu$  and  $qqqq$  decay channels are 84%, 84% and 86% respectively. This corresponds to a total efficiency of 85%. The selection efficiencies, broken down into the different lepton flavours are summarised in Table 2. For the data samples away from the  $W$ -pair threshold the selection efficiencies depend only weakly on centre-of-mass energy. The main features of the selections and associated systematic uncertainties are described below in Sects. 3.1–3.3.

**Table 2.** The luminosity-weighted average selection efficiencies for the CC03 processes for  $\sqrt{s} = 161\text{--}209$  GeV. The efficiencies include corrections for detector occupancy and tracking inefficiencies as described in the text. In the  $\ell\nu\ell\nu$  and  $qql\nu$  selections leptons from  $\tau$  decays are separated from direct leptons from  $W$ -decay on the basis of momentum and/or kinematic variables

Event selection	Efficiencies [%] for $W^+W^- \rightarrow$									
	$e\nu e\nu$	$\mu\nu\mu\nu$	$\tau\nu\tau\nu$	$e\nu\mu\nu$	$e\nu\tau\nu$	$\mu\nu\tau\nu$	$qqe\nu$	$qq\mu\nu$	$qq\tau\nu$	$qqqq$
$e\nu e\nu$	74.1	0.0	0.8	0.4	6.6	0.1	0.0	0.0	0.0	0.0
$\mu\nu\mu\nu$	0.0	77.9	0.7	1.4	0.1	6.7	0.0	0.0	0.0	0.0
$\tau\nu\tau\nu$	0.7	0.7	48.1	0.7	4.9	5.6	0.0	0.0	0.0	0.0
$e\nu\mu\nu$	2.6	0.4	1.4	76.5	6.2	6.9	0.0	0.0	0.0	0.0
$e\nu\tau\nu$	10.3	0.0	11.5	5.6	64.2	1.2	0.0	0.0	0.0	0.0
$\mu\nu\tau\nu$	0.2	9.5	8.4	4.3	0.8	61.5	0.0	0.0	0.0	0.0
$qqe\nu$	0.0	0.0	0.0	0.0	0.2	0.0	84.3	0.1	4.0	0.0
$qq\mu\nu$	0.0	0.0	0.0	0.0	0.0	0.1	0.2	88.3	4.4	0.1
$qq\tau\nu$	0.0	0.0	0.2	0.0	0.0	0.0	4.3	4.4	61.5	0.5
$qqqq$	0.0	0.0	0.0	0.0	0.0	0.0	0.0	0.1	0.8	85.9

### 3.1 Selection of $W^+W^- \rightarrow \ell\nu\ell\nu$ events

The  $W^+W^- \rightarrow \ell\nu\ell\nu$  process results in an event with two charged leptons, not necessarily of the same flavour, and significant missing momentum. This characteristic event topology is of interest both for measuring aspects of  $W$  physics and for exploring the potential production of new particles leading to the same experimental signature. The  $W^+W^- \rightarrow \ell\nu\ell\nu$  event selection described here first requires events to be selected by the general event selection used by OPAL to search for new particles such as pair production of super-symmetric particles which decay leptonically [38]. This selection identifies events consistent with there being two charged leptons and significant missing transverse momentum. From this sample cuts are applied to identify events consistent with being from the  $W^+W^- \rightarrow \ell\nu\ell\nu$  process. This event selection takes advantage of changes to the OPAL detector made in 1998. Consequently the data from centre-of-mass energies of 161 [3], 172 [4] and 183 GeV [1] have not been reanalysed.

The general  $\ell\nu\ell\nu$  event selection is described in detail in [38] and references therein. The selection is formed by requiring that an event be selected by either of two independent event selections, referred to in [38] as Selections I and II. Both event selections require evidence for significant missing transverse momentum and are designed to minimise background contributions from SM processes which can lead to an experimental signature of two charged leptons and significant missing transverse momentum. In the case of background processes, significant missing transverse momentum can arise from a number of sources: secondary neutrinos in tau decays; mis-measurement of the lepton energies and directions; or where high transverse momentum particles are incident on poorly instrumented regions of the detector.

Selection I is designed to retain efficiency for events with low visible energy. Selection II is designed for measuring  $W^+W^- \rightarrow \ell\nu\ell\nu$  events which have substantial visible energy; the selection criteria have been optimised to maximise the statistical power (efficiency multiplied by purity) treating CC03  $W^+W^- \rightarrow \ell\nu\ell\nu$  as signal and SM processes other than  $\ell\nu\ell\nu$  as background. For both Selections I and II particular care is taken to reject events with fake missing momentum due to detector effects. Neither selection attempts to reduce the sensitivity to non-CC03 sources of  $\ell\nu\ell\nu$  events with two detected leptons. There is a large overlap in the expected acceptance of the two selections: from the selected MC event sample, 6% of events are selected exclusively by Selection I and 6% exclusively by Selection II. Conversely, of the MC SM background events from processes other than  $\ell\nu\ell\nu$ , 9% pass both selections, 32% exclusively pass Selection I and 59% exclusively pass Selection II.

Both selections are cut-based and rather involved [38], and only an outline of the main points is given here. The most significant variables used are:  $x_{\min}$  ( $x_{\max}$ ), the momentum of the lower (higher) momentum charged lepton candidate scaled to the beam energy;  $x_T$ , the magnitude of the missing momentum scaled to the beam energy;  $\phi_{\text{acop}}$ , the supplement of the azimuthal opening angle;  $\theta_p^{\text{miss}}$ , the

polar angle of the missing momentum vector;  $p_z^{\text{miss}}$ , the magnitude of the  $z$  component of the missing momentum;  $a_T^{\text{miss}}$ , the component of the missing transverse momentum that is perpendicular to the event thrust axis in the transverse plane; and  $\theta_a^{\text{miss}} = \tan^{-1}[a_T^{\text{miss}}/p_z^{\text{miss}}]$ .

Selection I is based on three main requirements:

- evidence that a pair of charged leptons is produced, where at least one must have  $p_T$  exceeding 1.5 GeV and must satisfy requirements on lepton identification and isolation;
- evidence of statistically significant missing transverse momentum. For large acoplanarity events,  $\phi_{\text{acop}} > \pi/2$ ,  $x_T$  is required to exceed 0.045. For  $\phi_{\text{acop}} < \pi/2$ , i.e. events where the leptons are more back-to-back, a combination of cuts on  $x_T$ ,  $a_T^{\text{miss}}$  and  $\theta_a^{\text{miss}}$  is used. The cuts depend on the di-lepton identification information;
- a veto on events with apparent missing transverse momentum caused by poorly reconstructed low-angle particles in the forward region of the detector.

Selection I is designed as a general selection for di-lepton events with missing transverse momentum. In order to isolate events consistent with the process  $W^+W^- \rightarrow \ell\nu\ell\nu$ , additional cuts are applied in this analysis to remove events which have relatively low missing transverse momentum (an important region for SUSY and other new particle searches but not for  $W$ -pair production):

- events are rejected if  $x_{\max} < 0.1$ ;
- if  $x_T < 0.2$ ,  $|\cos \theta_p^{\text{miss}}| > 0.7$  and  $x_{\min} < 0.3$ , events are rejected if either  $x_{\max} < 0.15$  or  $\phi_{\text{acop}} < \pi/2$  and  $\theta_a^{\text{miss}} < 0.1$ ;
- for events with only one reconstructed isolated charged lepton candidate, events are rejected if the net momentum of the additional tracks and clusters not associated to the lepton divided by their invariant mass is less than 4.

Selection II starts from a preselected sample of low multiplicity events and makes little use of lepton identification information in the event selection procedure. The first stage of the selection is to apply a cone jet-finding algorithm [39] using a cone half-opening angle of  $20^\circ$  and a jet energy threshold of 2.5 GeV. The majority (90%) of  $W^+W^- \rightarrow \ell\nu\ell\nu$  events are reconstructed in the di-jet category. For events reconstructed as two jet events, the three most important selection criteria are:

- evidence for missing transverse momentum defined by requiring that  $x_T$  should exceed 0.05 by greater than one standard deviation;
- for low acoplanarity events  $a_T^{\text{miss}}$  should exceed 0.020, primarily to reject events where the missing momentum arises from secondary neutrinos from tau decays in  $e^+e^- \rightarrow \tau^+\tau^-$  events;
- a veto on activity in the forward region similar to Selection I.

Additional selections targeted at three-jet events (often  $W^+W^- \rightarrow \ell\nu\ell\nu\gamma$ ) and single jet events (one observed lepton plus evidence for the presence of another lepton) are used to improve the overall selection efficiency.

Events are classified as one of the six possible di-lepton types. For events selected by Selection II, the event classification uses both particle identification information and kinematic information as described in [2]. For events selected exclusively by Selection I the di-lepton classification is based on the lepton identification information only.

### 3.1.1 $W^+W^- \rightarrow \ell\nu\ell\nu$ selection systematic uncertainties

*Efficiency uncertainties.* The OPAL trigger and pretrigger systems provide a highly redundant and efficient trigger for  $W^+W^- \rightarrow \ell\nu\ell\nu$ ; studies indicate that the trigger inefficiency for events selected by these event selections is negligible. The  $W^+W^- \rightarrow \ell\nu\ell\nu$  event selection efficiencies are limited mainly by the geometrical acceptance of the detector and the defined kinematic acceptance. The latter is implicit in the requirement that the observed final state particles have a net visible transverse momentum which significantly exceeds that which could be explained by undetected particles at low polar angles. The detector acceptance is well understood and factors affecting the kinematic acceptance such as momentum and energy scales and resolutions are adequately modelled by the MC simulation. Extensive studies have been carried out comparing distributions of the event selection variables in data with MC. In general, reasonable agreement is found and quantitative estimates of the individual systematic effects are small compared to the statistical errors. In particular, the critical distributions associated with requiring missing transverse momentum, such as the  $a_T^{\text{miss}}$  and the  $x_T$  distributions are well modelled. As an example, the single most important cut in the two “jet” part of Selection II is the cut on  $a_T^{\text{miss}}$  which leads to a relative loss in the  $W^+W^- \rightarrow \ell\nu\ell\nu$  efficiency of 1.1%. A conservative estimate of the systematic error on the  $a_T^{\text{miss}}$  scale of 1% leads to a systematic uncertainty of 0.04% on the overall efficiency. As a result of such studies, an overall global event selection efficiency systematic uncertainty is assessed to be 5% of the fraction of signal events not identified by the selection (prior to occupancy corrections). This systematic uncertainty is taken to be fully correlated among centre-of-mass energies and ranges from 0.7% at 189 GeV to 0.8% at 207 GeV.

*Detector occupancy.* The  $W^+W^- \rightarrow \ell\nu\ell\nu$  event selection is sensitive to hits in the various sub-detectors which do not arise from the primary  $e^+e^-$  interaction, termed “detector occupancy”. Backgrounds from the accelerator, cosmic-ray muons, or electronic noise can lead to additional hits, energy deposition and even reconstructed tracks being superimposed on triggered data events. These detector occupancy effects are simulated by adding to the reconstructed MC events the hits, energy depositions and additional “jets” found in randomly triggered [40] beam-crossing data events corresponding to the same centre-of-mass energy. The detector occupancy corrections are included in the quoted efficiencies of Table 2. They reduce the overall efficiency and range from  $-0.4\%$  at 189 GeV to  $-1.0\%$  at 207 GeV. The variation is due to higher beam-related backgrounds at the highest energies. In order to take into account residual deficiencies in the implementation of these

post event reconstruction corrections, a systematic uncertainty amounting to one half of the correction is assigned.

The overall  $\ell\nu\ell\nu$  efficiency systematic uncertainties (for all final states combined) range from 0.8% to 1.0% for centre-of-mass energies of 189–209 GeV.

*Background uncertainties.* There are three main sources of background in the  $W^+W^- \rightarrow \ell\nu\ell\nu$  selection:

- **Non- $\ell\nu\ell\nu$  background:** Events from processes with no primary neutrinos which manage to fake the missing transverse momentum signature. Important sub-components are di-lepton production, in particular tau-pairs, multi-peripheral two-photon processes and the four-fermion  $e^+e^-f\bar{f}$  processes.
- **Non-interfering four-fermion background:**  $\ell\nu\ell\nu$  final states arising from processes such as  $ZZ$  with primary neutrinos in the final state and with lepton and neutrino flavours incompatible with  $WW$  production (e.g.  $\mu^+\mu^-\nu_\tau\bar{\nu}_\tau$ ).
- **Interfering four-fermion background:** The  $\ell\nu\ell\nu$  final states relevant to  $W^+W^- \rightarrow \ell\nu\ell\nu$  also have significant contributions from diagrams beyond those of CC03  $W$ -pair production, such as  $W\nu_e$ ,  $Ze^+e^-$ ,  $ZZ$  and  $Z\nu_e\bar{\nu}_e$ . These contributions, which can also interfere with the CC03 diagrams, are treated as an additive background.

For the centre-of-mass energy range  $\sqrt{s} = 161\text{--}209$  GeV, the luminosity-weighted average expected background cross sections are listed in Table 3.

The overall systematic uncertainties on the background cross sections for each di-lepton class and at each centre-of-mass energy are calculated by summing up the contributions in the following categories. The uncertainties within each category are assumed to be fully correlated among di-lepton channels and centre-of-mass energies.

- For events from di-lepton production the theoretical uncertainties are negligible. In this case it is simulation of the detector response that dominates the uncertainty on the background. Events are selected due to either mis-measurements of the variables used in the selection or from the tails of the  $\tau^+\tau^-$  decay distributions. An overall background systematic uncertainty of 10% is assessed.
- A 5% systematic uncertainty is assigned to the background expectations from genuine  $\ell\nu\ell\nu$  events coming both from non-interfering four-fermion background final states and from the non-CC03 contribution to final states where the four fermions are compatible with being from  $W$ -pair production.
- A 10% systematic uncertainty is assigned to the background expectations from  $e^+e^-f\bar{f}$  and the remaining small contributions from other four-fermion processes, reflecting the theoretical error on simulation of processes like  $Ze^+e^-$ .
- For events from the multi-peripheral  $e^+e^- \rightarrow e^+e^-X$  process an uncertainty of 30% is assigned. The uncertainty reflects the size of the discrepancy in the modelled number of events exclusively rejected using the forward scintillating tiles, a category of events dominated by multi-peripheral backgrounds.

**Table 3.** Luminosity-weighted average background cross sections [fb] in the different event selection categories. The background cross sections for the  $qq\tau\nu_\tau$  selection include the corrections described in the text. The quoted errors include both statistical and systematic uncertainties

Source of background	Background [fb] in selection									
	$e\nu e\nu$	$\mu\nu\mu\nu$	$\tau\nu\tau\nu$	$e\nu\mu\nu$	$e\nu\tau\nu$	$\mu\nu\tau\nu$	$qqe\nu$	$qq\mu\nu$	$qq\tau\nu$	$qqqq$
$l\nu l\nu$	20.0	17.0	18.0	21.0	31.0	17.0	0.0	0.0	0.0	0.0
$qq l\nu$	0.0	0.0	0.0	0.0	0.0	0.0	61.0	3.0	73.0	0.0
$qqqq$	0.0	0.0	0.0	0.0	0.0	0.0	0.0	1.0	6.0	493.0
$llll$	1.0	1.0	5.0	0.0	3.0	2.0	1.0	0.0	1.0	0.0
$qqll$	0.0	0.0	0.0	0.0	0.0	0.0	38.0	30.0	77.0	49.0
$qq\nu\nu$	0.0	0.0	0.0	0.0	0.0	0.0	1.0	1.0	36.0	0.0
$ll$	2.0	2.0	5.0	1.0	5.0	3.0	2.0	1.0	5.0	0.0
$qq$	0.0	0.0	0.0	0.0	0.0	0.0	41.0	23.0	78.0	1340.0
$e^+e^-X$	0.0	0.0	7.0	0.0	2.0	1.0	7.0	2.0	3.0	0.0
Total	23.0	21.0	35.0	23.0	41.0	23.0	152.0	63.0	280.0	1882.0
error	2.0	3.0	4.0	2.0	3.0	3.0	10.0	5.0	32.0	100.0

*Event classification uncertainties.* There are two aspects to the di-lepton flavour classification of selected  $W^+W^- \rightarrow l\nu l\nu$  candidates. Firstly, the algorithms for leptons to be identified as electrons, muons or hadronically decaying taus. These make use of many of the techniques of lepton identification used by OPAL in studies at the  $Z$ . Secondly, the kinematic re-classification algorithm based on scaled momentum which re-classifies soft leptons identified as electrons or muons as probable secondary leptons from taus, and uses electromagnetic calorimeter and muon information to re-assess whether highly energetic leptons initially not identified as electrons or muons are more consistent kinematically with prompt electrons or muons. The classification efficiency systematic uncertainty for genuine electrons and muons is assessed to be 2% based on the understanding of the lepton identification information in the large  $e^+e^- \rightarrow \ell^+\ell^-$  samples recorded at LEP1. The kinematic re-classification, which relies mainly on meas-

urement of the lepton energy, reduces the systematic uncertainties on the efficiencies for the individual final state lepton channels to the 1% level. In the extraction of the SM parameters that follows it has been verified that the effects of the  $l\nu l\nu$  classification systematic uncertainties are small. Nevertheless, the effects of the classification systematic uncertainties and correlations are included in the analysis.

### 3.1.2 $W^+W^- \rightarrow l\nu l\nu$ results

Using the KandY MC samples the luminosity-weighted average CC03  $W^+W^- \rightarrow l\nu l\nu$  event selection efficiency in the 189–209 GeV centre-of-mass energy range is estimated to be  $(84.7 \pm 0.8)\%$ . The inclusive selection efficiencies for the different centre-of-mass energies are listed in Table 4. The efficiencies for the different final states depend mostly on the number of taus present. The luminosity-

**Table 4.** Measured cross sections for the CC03 process  $e^+e^- \rightarrow W^+W^- \rightarrow l\nu l\nu$ . For the  $l\nu l\nu$  selection the data below  $\sqrt{s} = 188.63$  GeV have not been reanalysed and the results are taken from [1, 3, 4]. The errors on the cross sections are statistical and systematic. The numbers of selected events, the  $l\nu l\nu$  selection efficiencies and the expected numbers of background events are also listed. The backgrounds include a very small contribution from semi-leptonic  $W^+W^-$  decays which for the cross sections are taken to be fixed to their SM expectations

$\sqrt{s}$ [GeV]	$\mathcal{L}$ [ $\text{pb}^{-1}$ ]	$N$ [events]	Efficiency [%]	Background [events]	$\sigma(W^+W^- \rightarrow l\nu l\nu)$ [pb]	SM [pb]
161.30	9.9	2	$65.4 \pm 2.0$	$0.2 \pm 0.0$	$0.28 \pm 0.22 \pm 0.01$	0.38
172.11	10.4	8	$78.2 \pm 2.6$	$0.8 \pm 0.3$	$0.89 \pm 0.35 \pm 0.03$	1.28
182.68	57.4	78	$78.1 \pm 2.3$	$4.9 \pm 1.5$	$1.63 \pm 0.20 \pm 0.05$	1.62
188.63	183.0	295	$86.1 \pm 0.8$	$28.1 \pm 0.7$	$1.69 \pm 0.11 \pm 0.02$	1.72
191.61	29.3	56	$85.3 \pm 0.8$	$4.9 \pm 0.2$	$2.04 \pm 0.30 \pm 0.02$	1.75
195.54	76.4	145	$85.1 \pm 0.8$	$13.0 \pm 0.4$	$2.03 \pm 0.19 \pm 0.02$	1.78
199.54	76.6	138	$84.8 \pm 0.8$	$13.6 \pm 0.4$	$1.91 \pm 0.18 \pm 0.02$	1.79
201.65	37.7	86	$83.9 \pm 0.9$	$7.1 \pm 0.2$	$2.50 \pm 0.29 \pm 0.03$	1.80
204.88	81.9	141	$83.5 \pm 1.0$	$16.3 \pm 0.5$	$1.82 \pm 0.17 \pm 0.02$	1.81
206.56	138.5	239	$83.5 \pm 1.0$	$27.8 \pm 0.8$	$1.83 \pm 0.13 \pm 0.02$	1.81

weighted average efficiencies are 89.4%, 83.2% and 71.9% for final states with zero, one and two taus respectively. For the 189–209 GeV data the selection efficiency does not depend strongly on centre-of-mass energy. The luminosity weighted efficiencies of the  $W^+W^- \rightarrow \ell\nu\ell\nu$  selection for the individual channels are given in Table 2. The efficiencies/numbers of expected events in all tables include the detector occupancy corrections described above.

In total, 1188 events are selected as  $W^+W^- \rightarrow \ell\nu\ell\nu$  candidates compared to the SM expectation of  $1138 \pm 9$  (the numbers refer to the entire data set from 161–209 GeV). Figure 1 shows kinematic distributions for reconstructed  $W^+W^- \rightarrow \ell\nu\ell\nu$  event samples. The data distributions are in good agreement with the MC expectations. The numbers of selected  $\ell\nu\ell\nu$  events at each energy are used to determine the cross sections for  $e^+e^- \rightarrow W^+W^- \rightarrow \ell\nu\ell\nu$  given in Table 4. The measured cross sections are in agreement with the SM expectations.

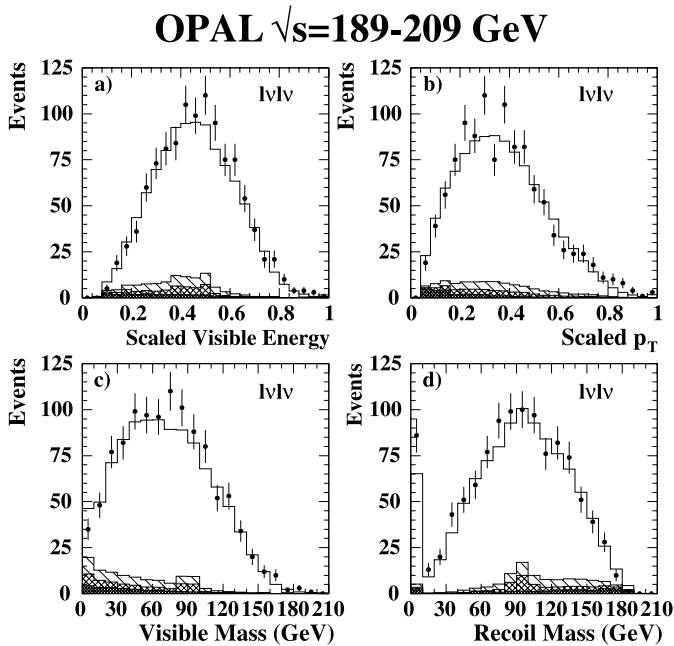


**Fig. 1.** For selected  $\ell\nu\ell\nu$  events the plots show distributions of **a** the total visible energy in the event scaled to the centre-of-mass energy, **b** the magnitude of the net visible transverse momentum in the event scaled to the beam energy, **c** the reconstructed total visible invariant mass of the event, and **d** the invariant mass of the system recoiling against the visible system. In **d** the events in the first bin are where the reconstructed recoil mass squared is negative. All plots show the selected  $\ell\nu\ell\nu$  events for the combined sample from data recorded at  $\sqrt{s} = 189\text{--}209$  GeV. The data are shown as the *points with error bars* (statistical errors only). The total standard model MC prediction is shown by the *unshaded histogram*. The background components are also shown: interfering  $\ell\nu\ell\nu$  (singly-hatched), non-interfering  $\ell\nu\ell\nu$  (cross-hatched) and two fermion/multi-peripheral (densely cross-hatched). The MC is normalised to the integrated luminosity of the data

### 3.2 Selection of $W^+W^- \rightarrow qq\ell\nu$ events

The  $W^+W^- \rightarrow qq\ell\nu$  selection consists of three separate selections, one for each type of semi-leptonic decay. Only those events which are not already selected as  $\ell\nu\ell\nu$  candidates are considered by these selections. For each of the  $W^+W^- \rightarrow qqe\nu_e$ ,  $W^+W^- \rightarrow qq\mu\nu_\mu$ , and  $W^+W^- \rightarrow qq\tau\nu_\tau$  event selections, the main part is a relative likelihood method to reject the potentially large  $e^+e^- \rightarrow qq$  background. In the first stage, the  $W^+W^- \rightarrow qqe\nu_e$  and  $W^+W^- \rightarrow qq\mu\nu_\mu$  likelihood selections are performed. The  $W^+W^- \rightarrow qq\tau\nu_\tau$  likelihood selection is only applied to those events which have not already been selected. Finally, events passing either the  $W^+W^- \rightarrow qqe\nu_e$  or the  $W^+W^- \rightarrow qq\mu\nu_\mu$  selections may then be reclassified as  $W^+W^- \rightarrow qq\tau\nu_\tau$  candidates.

The  $W^+W^- \rightarrow qq\ell\nu$  event selections used here are almost identical to those described in previous Opal publications [1, 2]. However, using the entire Opal  $W^+W^-$  data has resulted in an improved understanding of the selection efficiencies and backgrounds. Using the improved estimates of the systematic uncertainties, the cut on the relative likelihood variable used to select  $qq\tau\nu_\tau$  candidates was re-optimised to minimise the total uncertainty (statistical and systematic) for this channel. As a result the cut on the likelihood was raised from 0.5 to 0.8 which reduces the efficiency by about 5%. This loss in efficiency is more than compensated by the factor of two reduction in background and the corresponding reduction in the associated systematic uncertainties.

#### 3.2.1 Event selection

The  $W^+W^- \rightarrow qq\ell\nu$  event selection utilises the distinct topology of  $W^+W^- \rightarrow qq\ell\nu$  events; missing energy and a high energy (usually isolated) lepton. The selection consists of six stages, which can be summarised as:

- **Loose preselection:** a loose preselection to remove events with low multiplicity or little visible energy.
- **Lepton candidate identification:** identification of the observed track in the event which is most consistent with being from the leptonic decay of a W boson. Candidate lepton tracks are identified for each of the  $qqe\nu_e$ ,  $qq\mu\nu_\mu$  and  $qq\tau\nu_\tau$  hypotheses.
- **Preselection:** different sets of cuts are applied for  $W^+W^- \rightarrow qqe\nu_e$ ,  $W^+W^- \rightarrow qq\mu\nu_\mu$ , and  $W^+W^- \rightarrow qq\tau\nu_\tau$  to remove events clearly incompatible with being signal (e.g. events are rejected if the total visible energy in the event is less than 0.3 of the centre-of-mass energy).
- **Relative likelihood selection:** different relative likelihood selections are used to identify  $W^+W^- \rightarrow qqe\nu_e$ ,  $W^+W^- \rightarrow qq\mu\nu_\mu$ , and  $W^+W^- \rightarrow qq\tau\nu_\tau$  candidates. The probability density functions used in the likelihood selections are obtained from MC at the different centre-of-mass energies. The variables used are either related to the properties of the lepton candidate (e.g. the lepton energy and degree of isolation) or the kinematic properties of the event (e.g. the total visible energy and the magnitude of the missing momentum).



- **Decay classification:** identification of  $qq\tau\nu_\tau$  candidates from events which were originally selected as  $qqe\nu_e$  or  $qq\mu\nu_\mu$ .
- **Four-fermion background rejection:** rejection of four-fermion backgrounds  $qq\ell^+\ell^-$ ,  $W\nu_e$ ,  $Ze^+e^-$  and  $qq\nu\bar{\nu}$ .

The first four stages, described in detail in [4], are optimised for the rejection of the  $e^+e^- \rightarrow qq$  background which, for the centre-of-mass energies considered here, has an expected cross section of between four and seven times larger than the  $W$ -pair production cross section. The most important feature of the selection is the looseness of the identification of possible lepton candidates. For both the  $W^+W^- \rightarrow qqe\nu_e$  and  $W^+W^- \rightarrow qq\mu\nu_\mu$  selections the track which is most consistent with being from a leptonic  $W$ -decay is identified. The lepton track identification is based on an absolute likelihood taking into account momentum, isolation and lepton identification variables. To avoid associated systematic uncertainties only very loose cuts are placed on the lepton identification likelihood. The lepton identification likelihood is then used as one of the input variables in the likelihood event selection. In this way the presence of *either* a good isolated lepton candidate or significant missing transverse momentum is usually sufficient for an event to be selected. This redundancy leads to high efficiency and reduces the dependence of the selection on the detailed simulation of the events and, consequently, leads to relatively small systematic uncertainties.

Because of the limited use of lepton identification information, approximately 33% of  $W^+W^- \rightarrow qq\tau\nu_\tau$  events are accepted by at least one of the  $qqe\nu_e$  and  $qq\mu\nu_\mu$  likelihood selections. In addition, approximately 4% of the  $W^+W^- \rightarrow qqe\nu_e$  and  $W^+W^- \rightarrow qq\mu\nu_\mu$  events pass both the  $qqe\nu_e$  and  $qq\mu\nu_\mu$  likelihood selections. Such events usually result from there being a genuine electron from a  $W$ -boson decay and a track from one of the jets being tagged as muon-like, or vice versa. Consequently additional likelihood selections, based primarily on lepton identification variables and track momentum, are used to categorise events passing the  $qqe\nu_e$  and  $qq\mu\nu_\mu$  likelihood selections into the three possible leptonic  $W$ -decay modes. The largest systematic uncertainties in the efficiencies for selecting  $W^+W^- \rightarrow qq\ell\nu$  events are associated with this step.

Only events which failed the  $W^+W^- \rightarrow qqe\nu_e$  and  $W^+W^- \rightarrow qq\mu\nu_\mu$  likelihood are passed to the  $W^+W^- \rightarrow qq\tau\nu_\tau$  event selection. The  $W^+W^- \rightarrow qq\tau\nu_\tau$  event selection consists of separate selections for four possible tau decay signatures:  $\tau \rightarrow e\nu\nu$ ,  $\tau \rightarrow \mu\nu\nu$ , single prong hadronic decay modes and three prong hadronic decay modes. The main difference between these selections is the power of the variables used to identify possible tau decay products and the relative level of backgrounds. An event is considered a  $qq\tau\nu_\tau$  candidate if it passes any one of these four selections.

Because the  $W^+W^- \rightarrow qq\ell\nu$  likelihood selections are designed to reject the dominant  $e^+e^- \rightarrow qq$  background they have a significant efficiency for other four-fermion processes, e.g.  $qqe\nu_e$  final states produced by the sin-

gle  $W$  ( $W\nu_e$ ) diagrams and  $qq\ell^+\ell^-$  production (mainly via  $e^+e^- \rightarrow ZZ$ ). Additional four-fermion background rejection cuts are applied to events passing the likelihood selections to reduce backgrounds from these processes. The four-fermion background rejection consists of three separate parts. Cuts are applied to selected  $qqe\nu_e$  and  $qq\mu\nu_\mu$  candidates to reduce backgrounds from  $qqe^+e^-$  and  $qq\mu^+\mu^-$  final states where both leptons are observed in the detector. Because of the lack of a clear signature for a lepton in  $W^+W^- \rightarrow qq\tau\nu_\tau$  events, the selection places more weight on missing transverse energy to reject  $e^+e^- \rightarrow qq$ . Consequently the  $W^+W^- \rightarrow qq\tau\nu_\tau$  selection accepts approximately 40% of hadronically decaying single  $W$  events ( $W\nu_e \rightarrow qqe\nu_e$ ). In these events the electron is usually produced in the far forward region beyond the experimental acceptance and a fragmentation track is mis-identified as a  $\tau$  lepton decay product. To reduce this background, an additional likelihood selection is applied which separates  $W^+W^- \rightarrow qq\tau\nu_\tau$  from  $W\nu_e$ . This also rejects background from  $e^+e^- \rightarrow qq\nu\bar{\nu}$ . Background in the  $W^+W^- \rightarrow qqe\nu_e$  selection from the  $Ze^+e^-$  final state, where the  $Z$  decays hadronically and one electron is far forward, is reduced with two kinematic fits, the first using the hypothesis that the event is  $W^+W^- \rightarrow qqe\nu_e$  and the second using the  $Ze^+e^-$  hypothesis.

In addition to the likelihood selections, cut based selections are used to identify  $W^+W^- \rightarrow qqe\nu_e$  and  $W^+W^- \rightarrow qq\mu\nu_\mu$  events where the lepton track is either poorly reconstructed or is beyond the tracking acceptance. These ‘trackless’ selections require clear evidence of an electron or muon in the calorimeter or muon chambers consistent with the kinematics of a  $W^+W^- \rightarrow qq\ell\nu$  event, without explicitly demanding a reconstructed track. These additional selections improve the overall efficiency by approximately 3% (5%) for  $W^+W^- \rightarrow qqe\nu_e$  ( $W^+W^- \rightarrow qq\mu\nu_\mu$ ) events, and more importantly result in a reduction in the systematic uncertainties associated with the modelling of the forward tracking acceptance.

### 3.2.2 Systematic uncertainties

Table 5 lists the various contributions to the systematic uncertainty on the  $qqe\nu_e$ ,  $qq\mu\nu_\mu$  and  $qq\tau\nu_\tau$  selection efficiencies. Many of the potential systematic effects primarily affect the classification of selected  $qq\ell\nu$  events rather than the overall  $qq\ell\nu$  efficiency. Amongst the effects studied were:

- i) Finite MC statistics of the KandY MC samples used to determine the efficiencies.
- ii) The fragmentation and hadronisation systematic uncertainties are studied with fully simulated MC  $W^+W^- \rightarrow qq\ell\nu$  samples where the hadronisation process is modelled using Jetset, Herwig or Ariadne. In addition, the parameters  $\sigma_q$ ,  $b$ ,  $\Lambda_{\text{QCD}}$ , and  $Q_0$  of the Jetset fragmentation model are varied by one standard deviation about their tuned values [17].
- iii) The largest single systematic uncertainty in the  $qq\ell\nu$  selection is due to an identified deficiency in the MC simulation of isolated tracks from the fragmentation/hadronisation process. Such tracks, if sufficiently iso-

**Table 5.** Sources of uncertainty on the  $W^+W^- \rightarrow qq\ell\nu$  selection efficiencies. The errors quoted apply to the selection efficiency for the combined  $\sqrt{s} = 183\text{--}209$  GeV data set. Entries where the systematic error estimate is less than 0.01% are denoted by “–”. The errors on the combined  $qq\ell\nu$  selection take into account correlations between the separate channels

Source of uncertainty	Signal efficiency error (%)			
	Event selection $W^+W^- \rightarrow$			
	$qqe\nu_e$	$qq\mu\nu_\mu$	$qq\tau\nu_\tau$	$qq\ell\nu$
i) MC statistics	0.07	0.06	0.10	0.04
ii) WW fragmentation	0.25	0.20	0.50	0.20
iii) Tau candidate ID	–	–	0.60	0.20
iv) $\mathcal{O}(\alpha)$ QED/electroweak	0.09	0.05	0.03	0.04
v) ISR and FSR	0.07	0.12	0.10	0.03
vi) ECAL energy response	0.11	–	0.08	0.03
vii) Track momentum response	0.07	0.05	0.08	0.02
viii) Jet energy response	0.01	–	0.02	0.01
ix) Tracking losses	0.30	0.05	0.06	0.10
x) Detector occupancy	0.03	0.03	0.06	0.03
xi) Preselection	0.10	0.10	0.15	0.12
xii) Likelihood selection	0.30	0.10	0.40	0.10
Other	0.04	0.03	0.02	0.03
Total	0.54	0.30	0.91	0.36

lated can have similar properties to those from hadronic tau decays. In data there is a clear excess of low momentum tracks which have been identified as the best tau decay candidate compared to the MC expectation. This excess persists at all stages in the event selection; for example, there is a  $\sim 10\%$  excess of data events passing the  $W^+W^- \rightarrow qq\tau\nu_\tau$  preselection cuts (a sample dominated by background from  $e^+e^- \rightarrow qq$ ). To assess the impact on the  $qq\tau\nu_\tau$  analysis, a control sample of two jet events is formed by removing the tracks and calorimeter clusters associated with the lepton in selected  $qqe\nu_e$  and  $qq\mu\nu_\mu$  events. The full  $qq\tau\nu_\tau$  event selection is applied to these events and the selection efficiency is found to be  $7.3 \pm 4.6\%$  higher in data than the MC expectation. Again there is a clear excess ( $25 \pm 7\%$ ) of isolated tracks with momenta less than 5 GeV. This data sample is used to provide a momentum dependent correction factor which is used to reweight all MC events where a fragmentation track is identified as the best tau candidate. After applying this correction, the data/MC agreement at all stages in the  $qq\tau\nu_\tau$  selection is significantly improved. The effect of this correction is to increase the expected background from  $qq\nu\bar{\nu}$  and single- $W$  ( $W\nu_e$ ) events. Because  $qq\tau\nu_\tau$  events can also be selected on the basis of a fragmentation track, the predicted selection efficiency for  $qq\tau\nu_\tau$  events is also increased by 0.6%. The full size of the corrections to efficiency and background are assigned as (correlated) systematic errors in the  $qq\tau\nu_\tau$  selection.

iv) The selection efficiencies are sensitive to hard photon radiation in the  $W$ -pair production process. The Opal data are consistent with the predictions from KandY [41]. Potential systematic biases are estimated by reweighting the KandY MC samples so as to turn off

the  $\mathcal{O}(\alpha)$  electroweak treatment of radiation from the  $W$ -bosons.

- v) A conservative estimate of the possible biases arising from FSR from the lepton or tau decay products is investigated by reweighting the MC so as to change the rate of such FSR by  $\pm 50\%$ . This mainly affects the classification of selected events. The selection efficiencies are found to be insensitive to the detailed treatment of ISR.
- vi), vii) and viii) Uncertainties in the detector calibration, linearity of energy response and MC simulation of the energy resolution were studied in detail for the Opal analysis of the  $W$ -boson mass [42]. The uncertainties related to ECAL energy, track momentum and jet energy response described therein are propagated to the event selection.
- ix)  $Z \rightarrow \ell^+\ell^-$  events are used to study the tracking efficiency for electrons and muons. It is found that the MC overestimates the efficiency for reconstructing electron and muon tracks in the forward region,  $|\cos\theta| > 0.9$ . The effect on the selection efficiency is reduced by a factor of approximately three due to the trackless selections. The MC efficiency estimates are corrected and the full size of the correction is assigned as a systematic error.
- x) Randomly triggered events recorded throughout the data-taking period are used to assess the impact of energy deposits in the detector (particularly in the forward luminosity calorimeters) which can result in the event being vetoed. As a result, the MC efficiencies were corrected and half the correction assigned as a systematic uncertainty.
- xi) The event preselection cuts remove approximately 1% of  $qq\ell\nu$  events. Possible systematic effects specifically

associated with the preselection (in addition to those described above) are studied applying the likelihood selection to all events failing just one of the preselection cuts. There is no evidence of any systematic bias and the statistical precision of the study is used to assign the systematic uncertainty.

- xii) The MC expectation for each of the variables used in the likelihood selection is compared to the observed distribution for the selected events. The ratio of data to MC is used to define bin-by-bin corrections for each distribution. These corrections are propagated back into the likelihood selection and the associated systematic errors are obtained from the resulting changes in the selection efficiencies.

*Background uncertainties.* Table 3 shows the background cross sections and total uncertainties for the three  $qq\ell\nu$  selections. The largest contributions to the background in the  $qq\ell\nu$  selections are from the four fermion final states  $qqe\nu_e$ ,  $qq\ell^+\ell^-$  and  $qq\nu\bar{\nu}$  and from  $e^+e^- \rightarrow qq$ . In the  $qq\tau\nu_\tau$  selection, the uncertainties on the four fermion backgrounds are dominated by the correction for isolated low momentum tracks described above. The  $qqe\nu_e$  background mainly arises from the single  $W$  process (including interference with the CC03 diagrams); a 5% uncertainty on this cross section is assumed [37]. Background from the  $e^+e^- \rightarrow qq$  process mainly arises from radiative return events with an unobserved photon in the beam direction where a hadronisation track is mis-identified as the lepton. The  $e^+e^- \rightarrow qq$  background is assigned a 10% systematic uncertainty for the MC modelling of the hadronisation process (based on comparisons of Pythia, Herwig and Ariadne). The MC estimate of this background rate is checked using control samples constructed from the data directly. For the background, ‘fake’ events are constructed by boosting hadronic  $Z$  events recorded at  $\sqrt{s} = 91$  GeV to the invariant mass distribution expected of quark pairs at the appropriate  $\sqrt{s}$ . There is an additional 11% uncertainty

on the  $e^+e^- \rightarrow qq$  background in the  $qqe\nu_e$  selection from uncertainties in the rate at which high energy photon conversions fake an electron. The backgrounds from multi-peripheral two photon processes (almost entirely from hadronic final states rather than from  $e^+e^- \rightarrow e^+e^-\ell^+\ell^-$ ) are assigned a systematic uncertainty of 50% to cover the variation in predictions obtained from different generators.

### 3.2.3 $W^+W^- \rightarrow qq\ell\nu$ results

Using the KandY MC samples the inclusive  $qq\ell\nu$  selection is estimated to be  $83.8 \pm 0.4\%$  efficient for  $W^+W^- \rightarrow qq\ell\nu$  events. The selection efficiencies for the different centre-of-mass energies are listed in Table 6. Above the  $W^+W^-$  threshold region the selection efficiency does not depend strongly on the centre-of-mass energy. The luminosity weighted efficiencies of the  $W^+W^- \rightarrow qq\ell\nu$  selection for the individual channels are given in Table 2. The efficiencies/numbers of expected events in all tables include small corrections (0.1%–0.3%) which account for tracking losses which are not modelled by the MC simulation of the OPAL detector. The effect of detector occupancy from beam-related backgrounds is also included as is the small correction associated with the identification of tau candidates described above.

In total 4572 events are selected as inclusive  $W^+W^- \rightarrow qq\ell\nu$  candidates in agreement with the SM expectation of  $4622 \pm 28$ . Figure 2 shows distributions of the reconstructed energy of the lepton in the  $qqe\nu_e$ ,  $qq\mu\nu_\mu$ , and  $qq\tau\nu_\tau$  selections and the summed distribution. The data distributions are in good agreement with the MC expectations.

The numbers of selected  $qq\ell\nu$  events at each energy are used to determine the cross sections for  $e^+e^- \rightarrow W^+W^- \rightarrow qq\ell\nu$  given in Table 6. The results are obtained assuming the small backgrounds from  $\ell\nu\ell\nu$  and  $qqqq$  are given by the SM. The measured cross sections are in agreement with the SM expectations.

**Table 6.** Measured cross sections for the process  $e^+e^- \rightarrow W^+W^- \rightarrow qq\ell\nu$ . For the  $qq\ell\nu$  selection the data below  $\sqrt{s} = 182.68$  GeV have not been reanalysed and the results are taken from [3, 4]. The errors on the cross sections are statistical and systematic respectively. The numbers of selected events,  $qq\ell\nu$  selection efficiencies and expected numbers of background events are also listed. The backgrounds include fully-leptonic and fully-hadronic  $W^+W^-$  decays for which the cross sections are taken to be their SM expectations

$\sqrt{s}$ [GeV]	$\mathcal{L}$ [ $\text{pb}^{-1}$ ]	$N$ [events]	Efficiency [%]	Background [events]	$\sigma(W^+W^- \rightarrow qq\ell\nu)$ [pb]	SM [pb]
161.30	9.9	12	$63.6 \pm 2.5$	$1.4 \pm 0.5$	$1.68 \pm 0.55 \pm 0.07$	1.58
172.11	10.4	55	$84.2 \pm 1.0$	$4.6 \pm 0.8$	$5.77 \pm 0.85 \pm 0.07$	5.31
182.68	57.4	357	$84.2 \pm 0.4$	$22.1 \pm 2.1$	$6.93 \pm 0.39 \pm 0.05$	6.74
188.63	183.0	1171	$84.6 \pm 0.4$	$89.8 \pm 5.7$	$6.98 \pm 0.22 \pm 0.05$	7.13
191.61	29.3	176	$84.6 \pm 0.4$	$15.1 \pm 1.0$	$6.48 \pm 0.54 \pm 0.05$	7.26
195.54	76.4	554	$84.1 \pm 0.4$	$43.6 \pm 2.6$	$7.94 \pm 0.37 \pm 0.05$	7.38
199.54	76.6	494	$83.7 \pm 0.4$	$44.8 \pm 2.7$	$7.01 \pm 0.35 \pm 0.05$	7.46
201.65	37.7	255	$83.6 \pm 0.4$	$22.1 \pm 1.3$	$7.39 \pm 0.51 \pm 0.05$	7.48
204.88	81.9	523	$83.9 \pm 0.4$	$52.3 \pm 3.2$	$6.85 \pm 0.33 \pm 0.05$	7.50
206.56	138.5	975	$83.6 \pm 0.4$	$86.9 \pm 5.1$	$7.67 \pm 0.27 \pm 0.05$	7.51

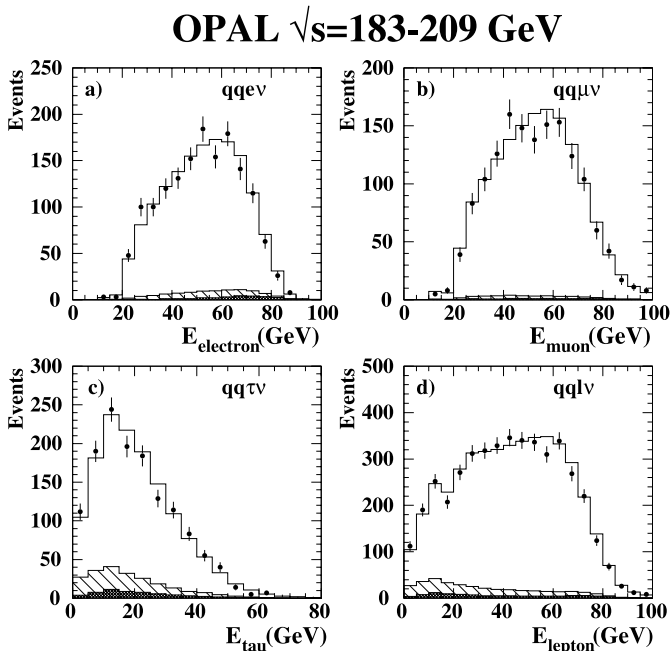


**Fig. 2.** Distributions of measured energies of the electrons, muons and visible tau decay products for events selected as  $qqe\nu$ ,  $qq\mu\nu$ , and  $qq\tau\nu$  respectively. The combined distribution for all events selected as  $qq\ell\nu$  is also shown. The data are shown as the *points with statistical error bars*, while the *histogram* is the total MC expectation. The combined background from two-fermion and two-photon processes is shown by the *cross-hatched region*, while the non-CC03 four-fermion background is shown by the *single-hatched region*.

### 3.3 Selection of $W^+W^- \rightarrow qq\bar{q}\bar{q}$ events

The selection of fully hadronic  $W^+W^- \rightarrow qq\bar{q}\bar{q}$  events is performed in two stages using a cut-based preselection followed by a likelihood selection procedure. This likelihood selection is primarily designed to reject the dominant background from the  $e^+e^- \rightarrow qq$  process where the di-quark system fragments into a four jet topology. No attempt is made to discriminate against the neutral current process  $ZZ \rightarrow qq\bar{q}\bar{q}$  for which the cross section is at least an order of magnitude smaller than that for  $W^+W^- \rightarrow qq\bar{q}\bar{q}$ . The preselection and likelihood selection variables are unchanged from those described in previous OPAL publications [2] although the tuning of the likelihood discriminant is updated for different ranges of  $\sqrt{s}$ .

#### 3.3.1 Event selection

All events which are classified as hadronic [43] and which have not been selected by either the  $l\nu l\nu$  or the  $qq\ell\nu$  selections are considered as candidates for the  $W^+W^- \rightarrow qq\bar{q}\bar{q}$  selection. In addition, any event which is identified and rejected as a four-fermion background event in the  $qq\ell\nu$  selection is also rejected as a  $qq\bar{q}\bar{q}$  candidate event.

Tracks and calorimeter clusters are combined into four jets using the Durham algorithm [44–47] and the total momentum and energy of each jet is corrected for double-

counting of energy [48]. To remove events which are clearly inconsistent with a fully hadronic  $W^+W^-$  decay, candidate events are required to satisfy a set of preselection cuts including a cut on minimum visible energy (70% of  $\sqrt{s}$ ), minimum invariant mass (75% of  $\sqrt{s}$ ), and minimum multiplicity per jet (one track). The most important preselection cut is  $\log_{10}(W_{420}) < 0$  [49], where  $W_{420}$  is the QCD matrix element calculated as an event weight formed from the tree level  $\mathcal{O}(\alpha_s^2)$  matrix element [50] for the four jet production processes ( $e^+e^- \rightarrow qq \rightarrow qq\bar{q}\bar{q}, qq\bar{q}\bar{q}$ ). The value of  $W_{420}$  is determined by using the observed momenta of the four reconstructed jets as estimates of the underlying parton momenta which are input to the matrix element calculation. The best discriminating power between signal and background was found using a variable defined as the largest value of the  $W_{420}$  matrix element from any of the 24 possible jet-parton associations in each event.

The preselection requirements reject around 95% of the  $e^+e^- \rightarrow qq$  events which comprise the dominant source of background in the  $W^+W^- \rightarrow qq\bar{q}\bar{q}$  event selection, while the preselection efficiency for the hadronic  $W^+W^- \rightarrow qq\bar{q}\bar{q}$  decays is estimated to be 90%–93% depending on  $\sqrt{s}$ .

Events satisfying the preselection cuts are classified as signal or background based upon a four variable likelihood selection. The following likelihood variables are selected to provide a good separation between the hadronic  $W^+W^- \rightarrow qq\bar{q}\bar{q}$  signal and the  $e^+e^- \rightarrow qq$  four jet background, while minimising the total number of variables used:

- $\log_{10}(W_{420})$ , the QCD four jet matrix element;
- $\log_{10}(W_{\text{CC03}})$ , the Excalibur matrix element [51] for the CC03 process ( $W^+W^- \rightarrow qq\bar{q}\bar{q}$ );
- $\log_{10}(y_{45})$ , the logarithm of the value of the Durham jet resolution parameter at which an event is reclassified from four jets to five jets;
- event sphericity.

Figure 3 shows the distribution of these four likelihood variables for all preselected events found in the 183–209 GeV data. To improve the statistical power of this selection, a multi-dimensional likelihood technique is used to account for the correlations between the four likelihood input variables [52]. Most of the separation between the signal and background events is provided by the two matrix element values  $\log_{10}(W_{\text{CC03}})$  and  $\log_{10}(W_{420})$ , which is related to the relative probability that the kinematics of the observed event are consistent with signal or background production respectively. While the likelihood input variables are the same for events in all  $\sqrt{s}$  ranges, the likelihood discriminant functions are separately calculated from CC03 signal and  $e^+e^- \rightarrow qq$  background MC samples in three ranges of  $\sqrt{s}$ : 185–194 GeV, 194–202.5 GeV, and 202.5–209.0 GeV. Candidate events at  $\sqrt{s}$  below 185 GeV are unchanged from previous OPAL publications [1, 3, 4].

An event is selected as a hadronic  $W^+W^- \rightarrow qq\bar{q}\bar{q}$  candidate if the likelihood discriminant variable, also shown in Fig. 3, is greater than 0.4. This cut value was chosen to maximise the expected statistical power of this selection assuming the SM rate for CC03 production.

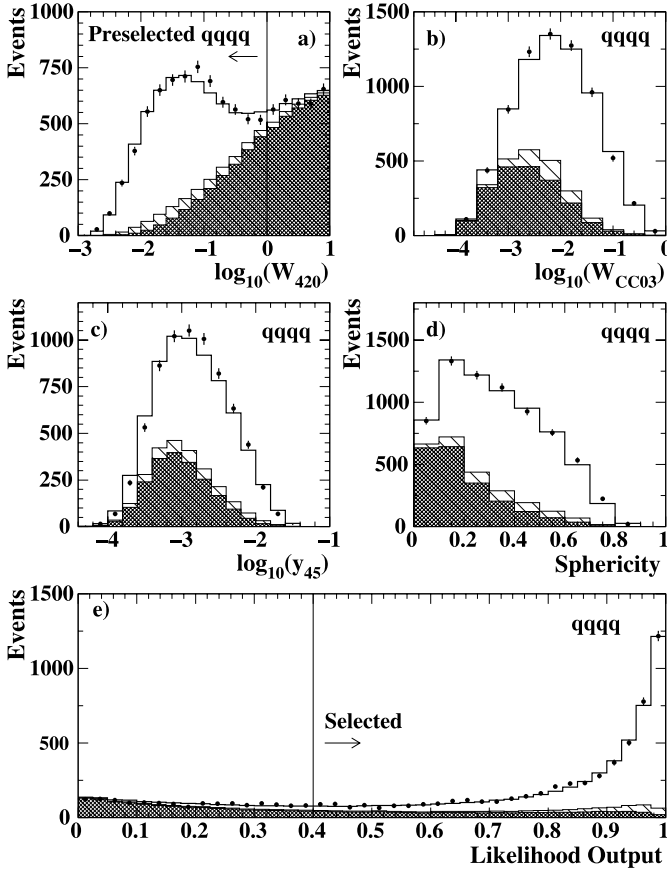


**Fig. 3.** Distributions of the variables (described in the text) used in the likelihood selection of  $W^+W^- \rightarrow qqqq$  events (a–d) and the resulting relative likelihood distribution (e). All plots are shown for the combined sample from data recorded between  $\sqrt{s} = 183\text{--}209$  GeV. The data are shown as the *points with error bars* (statistical errors only). The total standard model MC prediction is shown by the *unshaded histogram*. The background components are also shown: four-fermion background (*singly-hatched*) and two-fermion background (*cross-hatched*). The MC is normalised to the integrated luminosity of the data

### 3.3.2 Background estimation

The accepted  $e^+e^- \rightarrow qq$  background is estimated from KK2f MC samples, with Pythia, Herwig and Ariadne hadronisation being used as cross-checks. To reduce the uncertainty on this background estimate, a technique to measure this rate directly from the data is used. By comparing the number of events seen in data and MC in the range  $0 < \log_{10}(W_{420}) < 1$  which would otherwise pass the preselection cuts, the overall four jet background rate predicted by the MC is normalised to the observed data. This procedure is performed and applied separately in the three  $\sqrt{s}$  selection ranges described above. A luminosity-weighted average correction over the full  $\sqrt{s}$  range of  $(-1.4 \pm 1.7)\%$  is found for the default KK2f samples, where the uncertainty is the statistical precision of the normalisation procedure. The observed data and corrected MC expectation in this sideband background region are shown

in Fig. 3. The expected contamination from CC03 production in this region is less than 3%, resulting in a negligible bias on the extracted CC03 cross section.

### 3.3.3 Selection uncertainties

The main systematic uncertainty on the selection efficiency results from the modelling of the QCD hadronisation process. This uncertainty is estimated by comparing the selection efficiency predicted using the Jetset hadronisation model with alternative models including Herwig, Ariadne and an older version of the OPAL Jetset tuning [53]. These variations cover the observed data/MC differences such as the  $y_{45}$  distribution shown in Fig. 3. The uncertainty in the selection efficiency from the modelling of the hadronisation process is almost exclusively due to the preselection requirements, and is found to be independent of  $\sqrt{s}$ . The largest observed deviation in selection efficiency is taken as the systematic uncertainty, resulting in an estimated relative uncertainty of 0.9% which is fully correlated between different  $\sqrt{s}$  samples.

Cross-checks of this uncertainty are performed by comparing the observed shapes of both the preselection and selection variables seen in data to those predicted by the signal MC samples. After subtracting the expected background, the differences between observed data and expected MC signal distributions are comparable to the variations observed within the different hadronisation models themselves. In addition, the effect of directly varying the parameters  $\sigma_q$ ,  $b$ ,  $\Lambda_{\text{QCD}}$ , and  $Q_0$  of the Jetset hadronisation model by one standard deviation about their tuned values [17] as was done for previous OPAL results [2] leads to similar uncertainties.

Additional uncertainties on the modelling of the underlying hard process are evaluated by comparing CC03 events produced by KandY with other generators (Excalibur, Pythia, and grc4f [54]). Uncertainties on the detector modelling are evaluated from direct comparison of data distributions with MC predictions, and are generally smaller than the observed differences seen between the different hadronisation models. Possible biases related to final state interactions between the hadronic systems produced by different W bosons have been evaluated for colour-reconnection effects [55–57] and Bose–Einstein correlations [58]. These effects are found to be small, and the total change in predicted selection efficiency when these effects are included in the hadronisation model is taken as the systematic uncertainty.

### 3.3.4 Background uncertainties

The dominant uncertainty on the expected background rate comes from the modelling of the hadronisation process, particularly in  $e^+e^- \rightarrow qq$  events. This uncertainty is evaluated in the same manner as the hadronisation uncertainty for the signal efficiency, using large MC samples produced with a variety of hadronisation models, and taking the largest observed deviation as an estimate of the systematic uncertainty. The background normalisation procedure has been consistently applied during these system-

atic checks. The uncertainty on the estimated background is about 75 fb (the exact value depends on the centre-of-mass energy) which is taken to be fully correlated between different  $\sqrt{s}$  samples. The uncertainty from modelling of the hadronisation process for the background estimation is found to be largely uncorrelated with the uncertainty on the signal efficiency.

The background normalisation procedure contributes an additional, statistical uncertainty to the background estimation of about 3% which is uncorrelated between different  $\sqrt{s}$  ranges. Additional uncertainties in the non-CC03 four-fermion background are estimated by comparing the expectations of KoralW, gr4f, and Excalibur. This background is predominantly from the neutral current process  $ZZ \rightarrow qq\bar{q}\bar{q}$ , of which only 20% is in final states with direct interference with the CC03 diagrams. In each case, the single largest difference observed in a set of systematic checks is taken as an estimate of the uncertainty.

### 3.3.5 $W^+W^- \rightarrow qq\bar{q}\bar{q}$ results

The luminosity-weighted efficiency of the likelihood selection for  $W^+W^- \rightarrow qq\bar{q}\bar{q}$  events is estimated from KandY MC samples to be  $85.9 \pm 0.9\%$ , where the error represents an estimate of the systematic uncertainties. A total of 5933  $W^+W^- \rightarrow qq\bar{q}\bar{q}$  candidate events are selected compared to the expectation of  $5845.2 \pm 67.5$ . The luminosity-weighted purity of the selected event sample is 77%. The selection efficiencies for the different centre-of-mass energies are listed in Table 7. For the 189–209 GeV data the selection efficiency does not depend strongly of centre-of-mass energy. The numbers of selected  $qq\bar{q}\bar{q}$  events at each energy are used to determine cross sections for  $e^+e^- \rightarrow W^+W^- \rightarrow qq\bar{q}\bar{q}$ , also listed in Table 7. The results are obtained assuming the small backgrounds from  $l\nu l\nu$  and  $q\bar{q}l\nu$  are given by the SM. The measured cross sections are in agreement with the SM expectations.

## 4 Measurement of the $W^+W^-$ cross section

The observed numbers of selected  $W^+W^-$  events are used to measure the  $W^+W^-$  production cross section and the  $W$  decay branching fractions to leptons and hadrons. The measured cross section corresponds to that of  $W$ -pair production from the CC03 diagrams as discussed earlier. The expected four-fermion backgrounds quoted throughout this paper include contributions from both non-CC03 final states and the effects of interference with the CC03 diagrams. Mis-identified CC03 final states are not included in the background values listed in Table 3, but rather are taken into account by off-diagonal entries in the efficiency matrix. Table 8 summarises the event selections in the ten  $W^+W^-$  decay topologies.

The  $W^+W^-$  cross section and branching fractions are measured using data from the ten separate decay channels. The physical parameters (cross sections, branching ratios, etc.) are obtained from fits where all correlated systematic uncertainties are taken into account. The total cross section is obtained from a maximum likelihood fit to the numbers of events in the ten decay channels from data at all centre-of-mass energies allowing the cross sections at each centre-of-mass energy to vary and assuming the SM branching fractions. Efficiency, background, and luminosity systematic uncertainties are included as nuisance parameters with Gaussian penalty terms in the likelihood function [59]. Correlations are accounted for in the covariance matrix of the nuisance parameters associated with the systematic uncertainties. The results are listed in Table 9 and shown in Fig. 4. In both cases the results are compared to the SM expectation which is taken to be the mean of the cross sections predicted by YfsWW and RacoonWW (on average the predicted cross section from YfsWW is 0.2% higher than that from RacoonWW). The results do not differ significantly if the SM branching fractions are left unconstrained in the fit.

**Table 7.** Measured cross sections for the process  $e^+e^- \rightarrow W^+W^- \rightarrow qq\bar{q}\bar{q}$ . For the  $qq\bar{q}\bar{q}$  selection the data below  $\sqrt{s} = 182.68$  GeV have not been reanalysed and the results are taken from [3, 4]. The errors on the cross sections are statistical and systematic respectively. The numbers of selected events,  $qq\bar{q}\bar{q}$  selection efficiencies and expected numbers of background events are also listed. The backgrounds include semi-leptonic  $W^+W^-$  decays which for the cross sections are taken to be fixed to their SM expectations

$\sqrt{s}$ [GeV]	$\mathcal{L}$ [ $\text{pb}^{-1}$ ]	$N$ [events]	Efficiency [%]	Background [events]	$\sigma(W^+W^- \rightarrow qq\bar{q}\bar{q})$ [pb]	SM [pb]
161.30	9.9	14	$56.7 \pm 3.5$	$3.4 \pm 0.4$	$1.88 \pm 0.67 \pm 0.14$	1.64
172.11	10.4	54	$70.3 \pm 3.0$	$13.1 \pm 1.9$	$5.62 \pm 1.01 \pm 0.24$	5.52
182.68	57.4	439	$86.3 \pm 0.9$	$98.1 \pm 6.8$	$6.89 \pm 0.42 \pm 0.11$	7.00
188.63	183.0	1553	$86.6 \pm 0.9$	$339.5 \pm 17.8$	$7.66 \pm 0.25 \pm 0.12$	7.41
191.61	29.3	245	$86.2 \pm 0.9$	$55.2 \pm 2.8$	$7.51 \pm 0.62 \pm 0.12$	7.54
195.54	76.4	709	$87.2 \pm 0.9$	$152.6 \pm 7.8$	$8.35 \pm 0.40 \pm 0.12$	7.67
199.54	76.6	643	$86.7 \pm 0.9$	$150.6 \pm 7.7$	$7.42 \pm 0.38 \pm 0.11$	7.75
201.65	37.7	342	$86.6 \pm 0.9$	$75.8 \pm 3.8$	$8.16 \pm 0.57 \pm 0.12$	7.77
204.88	81.9	683	$86.3 \pm 0.9$	$159.9 \pm 8.2$	$7.40 \pm 0.37 \pm 0.11$	7.79
206.56	138.5	1251	$86.1 \pm 0.9$	$274.4 \pm 13.9$	$8.19 \pm 0.30 \pm 0.12$	7.80

**Table 8.** Selected events in each of the 10  $W^+W^-$  decay topologies compared to the SM expectation. Also listed are the combined numbers for the six  $l\nu l\nu$  decay channels and for the three  $qq l\nu$  decay channels. The efficiencies and purities for the  $l\nu l\nu$  ( $qq l\nu$ ) decay channels are calculated treating all  $l\nu l\nu$  ( $qq l\nu$ ) events as signal; e.g. the quoted efficiencies in the  $l\nu l\nu$  channels represent the selected CC03 cross section for any  $l\nu l\nu$  flavour divided by the generated CC03 cross section in the specific channel. Note that the total ratio of data to MC is for the sum of signal and background events

Selection	Efficiency	Purity	Expected	Observed	Data/expected
$e\nu e\nu$	89.0%	88.1%	$136.7 \pm 2.4$	141	$1.032 \pm 0.087 \pm 0.018$
$\mu\nu\mu\nu$	95.0%	89.9%	$143.0 \pm 2.5$	156	$1.091 \pm 0.087 \pm 0.017$
$\tau\nu\tau\nu$	71.8%	79.5%	$122.2 \pm 3.4$	131	$1.072 \pm 0.094 \pm 0.028$
$e\nu\mu\nu$	91.8%	93.9%	$264.8 \pm 3.2$	251	$0.948 \pm 0.060 \pm 0.012$
$e\nu\tau\nu$	81.9%	88.5%	$250.5 \pm 4.2$	256	$1.022 \pm 0.064 \pm 0.017$
$\mu\nu\tau\nu$	75.6%	92.6%	$220.9 \pm 4.1$	253	$1.145 \pm 0.072 \pm 0.019$
$l\nu l\nu$	83.8%	89.7%	$1137.7 \pm 8.5$	1188	$1.044 \pm 0.030 \pm 0.007$
$qqe\nu$	88.3%	93.2%	$1597.5 \pm 9.8$	1585	$0.992 \pm 0.025 \pm 0.006$
$qq\mu\nu$	92.8%	96.8%	$1616.7 \pm 5.1$	1581	$0.978 \pm 0.025 \pm 0.003$
$qq\tau\nu$	70.1%	84.1%	$1407.8 \pm 23.6$	1406	$0.999 \pm 0.027 \pm 0.017$
$qq l\nu$	83.8%	91.7%	$4622.0 \pm 27.6$	4572	$0.989 \pm 0.015 \pm 0.006$
$qqqq$	85.9%	77.4%	$5845.2 \pm 67.5$	5933	$1.015 \pm 0.013 \pm 0.012$
Total	85.2%	84.7%	$11604.8 \pm 73.4$	11693	$1.008 \pm 0.009 \pm 0.006$

**Table 9.** Measured CC03  $W^+W^-$  cross sections from a combined fit to all data. The last column shows the SM expectations which are taken from the average of the predictions from YfsWW and RacoonWW

$\langle\sqrt{s}\rangle/\text{GeV}$	$\sigma_{WW}$ [pb]	$\sigma_{WW}^{\text{SM}}$ [pb]
161.30	$3.56 \pm 0.88 \pm 0.11$	3.61
172.11	$12.14 \pm 1.34 \pm 0.22$	12.10
182.68	$15.38 \pm 0.61 \pm 0.13$	15.37
188.63	$16.22 \pm 0.35 \pm 0.11$	16.26
191.61	$15.87 \pm 0.86 \pm 0.10$	16.55
195.54	$18.21 \pm 0.57 \pm 0.12$	16.82
199.54	$16.23 \pm 0.54 \pm 0.11$	17.00
201.65	$17.94 \pm 0.81 \pm 0.11$	17.05
204.88	$15.99 \pm 0.52 \pm 0.11$	17.10
206.56	$17.58 \pm 0.42 \pm 0.12$	17.12

When compared to the SM expectations, the 10 cross section measurements in Fig. 4 yield a  $\chi^2$  of 15.5 (11% probability). When the 100 individual event counts used to obtain the cross sections (ten channels  $\times$  ten  $\sqrt{s}$  bins) are compared to the SM expectation the  $\chi^2$  obtained is 94.5 for 100 degrees of freedom. The Opal  $W^+W^-$  data are consistent with the SM expectation. The cross sections listed in Table 9 differ from than the sums of the exclusive cross sections from the separate channels (listed in Tables 4, 6 and 7) because of the constraint to the SM branching ratios and the larger systematic errors in the  $qqqq$  channel.

A fit to the data where the expected cross sections at all centre-of-mass energies are given by the SM expectation

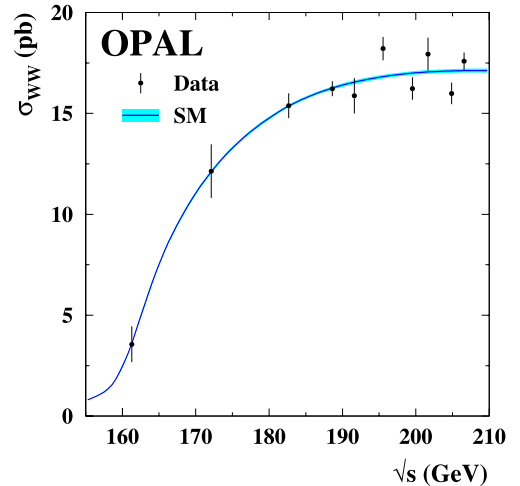


**Fig. 4.** The measured  $WW$  cross sections from fits assuming SM  $W$  decay branching fractions. The measured cross sections (*points*) are compared to the SM expectation (*line*) which is the average of the predictions from YfsWW and RacoonWW. The *shaded region* shows the 0.5% theoretical error

scaled by a single data/SM ratio gives:

$$\text{data/SM} = 1.002 \pm 0.011(\text{stat.}) \pm 0.007(\text{sys.}) \pm 0.005(\text{theory}),$$

where the SM expectation is the mean of the cross sections predicted by YfsWW and RacoonWW. It should be noted that the ratio in Table 8, which includes backgrounds, differs from this fit value due to: the constraint to the SM branching ratios; the larger systematic errors in the  $qqqq$

channel; and the different levels of background in the different decay channels.

## 5 Measurement of the $W$ branching fractions

A simultaneous fit to the numbers of  $W^+W^-$  candidate events in the ten identified final states ( $e\nu_e e\nu_e$ ,  $\mu\nu_\mu\mu\nu_\mu$ ,  $\tau\nu_\tau\tau\nu_\tau$ ,  $e\nu_e\mu\nu_\mu$ ,  $e\nu_e\tau\nu_\tau$ ,  $\mu\nu_\mu\tau\nu_\tau$ ,  $qqe\nu_e$ ,  $qq\mu\nu_\mu$ ,  $qq\tau\nu_\tau$ , and  $qqqq$ ) observed by OPAL at each of the ten centre-of-mass energies between 161 GeV and 207 GeV gives the following values for the leptonic branching fractions of the  $W$  boson:

$$\begin{aligned}\text{Br}(W \rightarrow e\nu_e) &= 10.71 \pm 0.25(\text{stat.}) \pm 0.11(\text{syst.})\% \\ \text{Br}(W \rightarrow \mu\nu_\mu) &= 10.78 \pm 0.24(\text{stat.}) \pm 0.10(\text{syst.})\% \\ \text{Br}(W \rightarrow \tau\nu_\tau) &= 11.14 \pm 0.31(\text{stat.}) \pm 0.17(\text{syst.})\%.\end{aligned}$$

Correlations between the systematic uncertainties at the different energy points have been accounted for in the fit as have correlations in the selection efficiency uncertainties for the different channels. These results are consistent with the hypothesis of lepton universality of the leptonic charged-current and agree well with the SM prediction of 10.83% [5]. The correlation coefficient for the resulting values of  $\text{Br}(W \rightarrow e\nu_e)$  and  $\text{Br}(W \rightarrow \mu\nu_\mu)$  is +0.14. The correlation coefficients for  $\text{Br}(W \rightarrow e\nu_e)$  and  $\text{Br}(W \rightarrow \mu\nu_\mu)$  with the measurement of  $\text{Br}(W \rightarrow \tau\nu_\tau)$  are -0.30 and -0.23 respectively. A simultaneous fit assuming lepton universality<sup>1</sup> gives

$$\text{Br}(W \rightarrow qq) = 67.41 \pm 0.37(\text{stat.}) \pm 0.23(\text{syst.})\%,$$

which is consistent with the SM expectation of 67.51%. Here, the largest single source of systematic uncertainty is that from the  $e^+e^- \rightarrow qq$  background in the  $W^+W^- \rightarrow qqqq$  channel.

Assuming the quark-lepton universality of the strength of the charged current weak interaction, the hadronic branching fraction can be interpreted as a measurement of the sum of the squares of the six elements of the CKM mixing matrix,  $|V_{ij}|$ , which do not involve the top quark:

$$\frac{\text{Br}(W \rightarrow qq)}{(1 - \text{Br}(W \rightarrow qq))} = \left(1 + \frac{\alpha_s(M_W)}{\pi}\right) \sum_{i=u,c; j=d,s,b} |V_{ij}|^2.$$

The theoretical uncertainty of this improved Born approximation due to missing higher order corrections is estimated to be 0.1% [5]. Taking  $\alpha_s(M_W)$  to be  $0.119 \pm 0.002$  [60], the branching fraction  $\text{Br}(W \rightarrow qq)$  from the 161–209 GeV data yields

$$\sum_{i=u,c; j=d,s,b} |V_{ij}|^2 = 1.993 \pm 0.033(\text{stat.}) \pm 0.023(\text{syst.}),$$

which is consistent with the value of 2 expected from unitarity in a three-generation CKM matrix. If one assumes

unitarity and a three-generation CKM matrix then this measurement can be interpreted as a test of quark-lepton universality of the weak coupling constant for quarks,  $g_W^{qq}$ , and for leptons,  $g_W^{\ell\nu}$ :

$$g_W^{qq}/g_W^{\ell\nu} = 0.996 \pm 0.017(\text{stat.}) \pm 0.011(\text{syst.}).$$

Finally, using the experimental measurements of the CKM matrix elements other than  $|V_{cs}|$  gives  $|V_{ud}|^2 + |V_{us}|^2 + |V_{ub}|^2 + |V_{cd}|^2 + |V_{cb}|^2 = 1.054 \pm 0.005$  [60], and the Opal result for  $\sum_{i=u,c; j=d,s,b} |V_{ij}|^2$  can be interpreted as a measurement of  $|V_{cs}|$  which is the least well determined of these matrix elements:

$$|V_{cs}| = 0.969 \pm 0.017(\text{stat.}) \pm 0.012(\text{syst.}).$$

The uncertainty in the sum of the other five CKM matrix elements, which is dominated by the uncertainty on  $|V_{cd}|$ , contributes a negligible uncertainty of 0.003 to this determination of  $|V_{cs}|$ .

## 6 $e^+e^- \rightarrow W^+W^-$ differential cross section

In  $qq\ell\nu$  events it is possible to reconstruct the polar angle of the produced  $W^-$  with respect to the  $e^-$  beam direction,  $\cos\theta_{W^-}$ , where the charge of the lepton tags the  $W^\pm$  and the jet momenta and the remaining event properties give the direction. Selected  $qqe\nu_e$  and  $qq\mu\nu_\mu$  events are used to measure the differential cross section,  $d(\sigma_{WW})/d(\cos\theta_{W^-})$ . Events selected solely by the trackless selections are not used here. Selected  $qq\tau\nu_\tau$  events are not considered due to the larger background and less reliable determination of lepton charge resulting from the possibility of the candidate tau being formed from tracks from the fragmentation of the quarks.

The measured  $qqe\nu_e$  and  $qq\mu\nu_\mu$  differential cross sections are corrected to correspond to the CC03 set of diagrams but with the additional constraint that, at generator level, the charged lepton is more than  $20^\circ$  away from the  $e^+e^-$  beam direction,  $20^\circ < \theta_{\ell^\pm} < 160^\circ$ . This angular requirement is closely matched to the experimental acceptance. It also greatly reduces the difference between the full four-fermion cross section and the CC03 cross section by reducing the contribution of  $t$ -channel single- $W$  diagram in the  $qqe\nu_e$  final state. At the MC generator level the angle  $\cos\theta_{W^-}$  is defined in terms of the four-momenta of the fermions from the  $W^-$  decay using the CALO5 photon recombination scheme [37]. The quoted differential cross sections correspond to  $d[\sigma(e^+e^- \rightarrow W^+W^- \rightarrow qqe\nu_e) + \sigma(e^+e^- \rightarrow W^+W^- \rightarrow qq\mu\nu_\mu)]/d\cos\theta_{W^-}$  within the above generator level acceptance.

The differential cross section is measured in ten bins of  $\cos\theta_{W^-}$  with the data divided into four  $\sqrt{s}$  ranges: 180.0–185.0 GeV; 185.0–194.0 GeV; 194.0–202.5 GeV; and 202.5–209.0 GeV. Experimentally the angle  $\cos\theta_{W^-}$  can be obtained from the measured momenta of the two jets with the lepton used to tag the charge of the  $W$  boson. However, to improve the angular resolution a kine-

<sup>1</sup> The effect of the tau mass, which results in a 0.1% fractional reduction in  $\text{Br}(W \rightarrow \tau\nu_\tau)$  [5], is neglected.



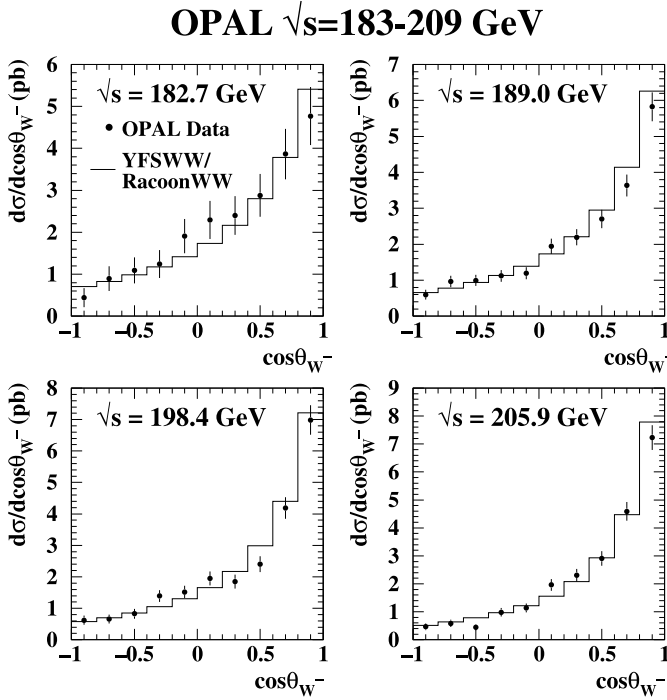


**Fig. 5.** The measured  $W^-$  polar angle differential cross section for  $qqe\nu$  and  $qq\mu\nu$  events within the acceptance defined in the text. The measurements are shown for the four energy bins described in the text. The measured cross sections (*points*) are compared to the theoretical expectations (*histograms*) from YfsWW and RacoonWW (indistinguishable on this scale)

matic fit to the four momenta of the two jets and the lepton is employed [42]. If the fit converges with a fit probability of  $> 0.1\%$  [42] the fitted jet momenta are used. If the kinematic fit yields a fit probability of  $< 0.1\%$ , which is the case for approximately 4% of  $qq\ell\nu$  events,  $\cos\theta_{W^-}$  is calculated from the measured jet four-momenta. From MC the  $\cos\theta_{W^-}$  resolution is found to be approximately 0.05.

**Table 10.** The measured differential cross section,  $d[\sigma(e^+e^- \rightarrow W^+W^- \rightarrow qqe\nu_e) + \sigma(e^+e^- \rightarrow W^+W^- \rightarrow qq\mu\nu_\mu)]/d\cos\theta_{W^-}$  expressed in ten bins of  $\cos\theta_{W^-}$  for the four centre-of-mass energy ranges. The cross sections correspond to the CC03 set of diagrams with the additional requirement that the charged lepton is more than  $20^\circ$  from the beam axis,  $20^\circ < \theta_{\ell^\pm} < 160^\circ$ . For each entry, the first uncertainty is statistical and the second systematic

$\cos\theta_{W^-}$ bin	Differential cross section [pb]			
	$\langle\sqrt{s}\rangle = 182.7$ GeV	$\langle\sqrt{s}\rangle = 189.0$ GeV	$\langle\sqrt{s}\rangle = 198.4$ GeV	$\langle\sqrt{s}\rangle = 205.9$ GeV
$-1.0 \rightarrow -0.8$	$0.44 \pm 0.22 \pm 0.02$	$0.60 \pm 0.14 \pm 0.03$	$0.62 \pm 0.15 \pm 0.04$	$0.46 \pm 0.12 \pm 0.04$
$-0.8 \rightarrow -0.6$	$0.90 \pm 0.30 \pm 0.02$	$0.97 \pm 0.16 \pm 0.02$	$0.66 \pm 0.15 \pm 0.02$	$0.59 \pm 0.13 \pm 0.02$
$-0.6 \rightarrow -0.4$	$1.09 \pm 0.31 \pm 0.01$	$1.00 \pm 0.16 \pm 0.01$	$0.83 \pm 0.15 \pm 0.01$	$0.44 \pm 0.11 \pm 0.02$
$-0.4 \rightarrow -0.2$	$1.24 \pm 0.33 \pm 0.01$	$1.12 \pm 0.17 \pm 0.01$	$1.39 \pm 0.19 \pm 0.01$	$0.98 \pm 0.15 \pm 0.01$
$-0.2 \rightarrow 0.0$	$1.91 \pm 0.41 \pm 0.01$	$1.19 \pm 0.17 \pm 0.01$	$1.52 \pm 0.20 \pm 0.01$	$1.14 \pm 0.16 \pm 0.01$
$0.0 \rightarrow +0.2$	$2.29 \pm 0.45 \pm 0.01$	$1.95 \pm 0.21 \pm 0.01$	$1.95 \pm 0.22 \pm 0.01$	$1.96 \pm 0.21 \pm 0.01$
$+0.2 \rightarrow +0.4$	$2.40 \pm 0.46 \pm 0.01$	$2.20 \pm 0.23 \pm 0.01$	$1.85 \pm 0.22 \pm 0.01$	$2.31 \pm 0.23 \pm 0.01$
$+0.4 \rightarrow +0.6$	$2.88 \pm 0.51 \pm 0.02$	$2.71 \pm 0.26 \pm 0.01$	$2.41 \pm 0.25 \pm 0.01$	$2.91 \pm 0.26 \pm 0.02$
$+0.6 \rightarrow +0.8$	$3.87 \pm 0.60 \pm 0.02$	$3.64 \pm 0.31 \pm 0.02$	$4.19 \pm 0.34 \pm 0.03$	$4.59 \pm 0.33 \pm 0.03$
$+0.8 \rightarrow +1.0$	$4.77 \pm 0.69 \pm 0.03$	$5.83 \pm 0.40 \pm 0.04$	$6.98 \pm 0.47 \pm 0.04$	$7.23 \pm 0.44 \pm 0.05$

The reconstructed  $\cos\theta_{W^-}$  distributions are corrected to the signal definition using the MC background estimates and a simple bin-by-bin efficiency correction. It has been verified that this simple bin-by-bin correction method is in good agreement with a more complete unfolding using the reconstructed to generator level migration.

The systematic uncertainties on the selection efficiencies and background cross sections described above are propagated to the differential cross section measurement. In addition it is known from studies of lepton pair production at LEP1 that the Opal MC underestimates the fraction of events where the lepton track is assigned the wrong charge [61]. This arises from imperfect tracking in the region of the jet chamber anode planes. For the data considered here the MC predicts that 0.5% of tracks are assigned the wrong charge. Based on previous studies [61] it is estimated that the corresponding number for data is  $(1.0 \pm 0.5)\%$ . In deriving the efficiency corrections, the MC reconstructed  $\cos\theta_{W^-}$  distributions are corrected for this difference and the full size of the correction is taken as the charge identification systematic uncertainty.

The measured differential cross sections in the 10 bins of  $\cos\theta_{W^-}$  for the four energy ranges are shown in Fig. 5 and the results are given in Table 10. The data are in good agreement with the SM expected generator level distributions obtained from either YfsWW or RacoonWW. Although the differential cross sections for these data have not been published previously, it should be noted that a deviation from the SM would have shown up in the OPAL triple gauge coupling analysis [62] which uses similar distributions.

## 7 Conclusions

From a total data sample of  $701.1 \text{ pb}^{-1}$  recorded with  $e^+e^-$  centre-of-mass energies of  $\sqrt{s} = 161\text{--}209$  GeV with the OPAL detector at LEP 11693  $W$ -pair candidate events are selected. The combined data samples is almost a fac-

tor three larger than the previous OPAL publication. This large sample of events has enabled a significant reduction in a number of systematic uncertainties compared with our previous publications.

The data are used to test the SM description of  $W^+W^-$  production in the centre-of-mass range  $\sqrt{s} = 161\text{--}209$  GeV. The  $W$ -pair production cross sections at 10 different centre-of-mass energies are found to be consistent with the standard model expectation:

$$\text{data/SM} = 1.002 \pm 0.011(\text{stat.}) \pm 0.007(\text{syst.}) \\ \pm 0.005(\text{theory}).$$

The data are then used to determine the  $W$  boson leptonic branching fractions:

$$\text{Br}(W \rightarrow e\nu_e) = 10.71 \pm 0.25(\text{stat.}) \pm 0.11(\text{syst.})\% \\ \text{Br}(W \rightarrow \mu\nu_\mu) = 10.78 \pm 0.24(\text{stat.}) \pm 0.10(\text{syst.})\% \\ \text{Br}(W \rightarrow \tau\nu_\tau) = 11.14 \pm 0.31(\text{stat.}) \pm 0.17(\text{syst.})\%.$$

These results are consistent with lepton universality of the charged current weak interaction and with the results of the other LEP collaborations [63–65]. Assuming lepton universality, the branching ratio to hadrons is determined to be  $67.41 \pm 0.37(\text{stat.}) \pm 0.23(\text{syst.})\%$  from which the CKM matrix element  $|V_{cs}|$  is determined to be  $0.969 \pm 0.017(\text{stat.}) \pm 0.012(\text{syst.})$ . The differential cross section as a function of the  $W^-$  production angle is measured for the  $qqe\nu$  and  $qq\mu\nu$  final states and found to be consistent with the SM expectation.

*Acknowledgements.* We particularly wish to thank the SL Division for the efficient operation of the LEP accelerator at all energies and for their close cooperation with our experimental group. In addition to the support staff at our own institutions we are pleased to acknowledge the Department of Energy, USA, National Science Foundation, USA, Particle Physics and Astronomy Research Council, UK, Natural Sciences and Engineering Research Council, Canada, Israel Science Foundation, administered by the Israel Academy of Science and Humanities, Benoziyo Center for High Energy Physics, Japanese Ministry of Education, Culture, Sports, Science and Technology (MEXT) and a grant under the MEXT International Science Research Program, Japanese Society for the Promotion of Science (JSPS), German Israeli Bi-national Science Foundation (GIF), Bundesministerium für Bildung und Forschung, Germany, National Research Council of Canada, Hungarian Foundation for Scientific Research, OTKA T-038240, and T-042864, The NWO/NATO Fund for Scientific Research, the Netherlands.

## References

1. OPAL Collaboration, G. Abbiendi et al., Eur. Phys. J. C **8**, 191 (1999)
2. OPAL Collaboration, G. Abbiendi et al., Phys. Lett. B **493**, 249 (2000)
3. OPAL Collaboration, K. Ackerstaff et al., Phys. Lett. B **397**, 147 (1997)
4. OPAL Collaboration, K. Ackerstaff et al., Eur. Phys. J. C **2**, 597 (1998)
5. Proceedings of the CERN LEP2 Workshop, CERN 96-01, Vols. 1 and 2, ed. by G. Altarelli, T. Sjöstrand, F. Zwirner
6. G. Aguillon, et al., Nucl. Instrum. Methods A **417**, 8 (1998)
7. OPAL Collaboration, K. Ahmet et al., Nucl. Instrum. Methods A **305**, 275 (1991)
8. B.E. Anderson et al., IEEE Trans. Nucl. Sci. **41**, 845 (1994)
9. S. Anderson et al., Nucl. Instrum. Methods A **403**, 326 (1998)
10. OPAL Collaboration, G. Abbiendi et al., Eur. Phys. J. C **13**, 553 (2000)
11. J. Allison et al., Nucl. Instrum. Methods A **317**, 47 (1992)
12. S. Jadach et al., Comput. Phys. Commun. **140**, 475 (2001) Program KORALW V1.53 and YFSWW3
13. D. R. Yennie, S. C. Frautschi, H. Suura, Ann. Phys. **13**, 379 (1961)
14. E. Barberio, Z. Was, Comput. Phys. Commun. **79**, 291 (1994)
15. T. Sjöstrand, Comput. Phys. Commun. **39**, 374 (1986)
16. T. Sjöstrand, M. Bengtsson, Comput. Phys. Commun. **43**, 367 (1987)
17. Opal Collaboration, G. Alexander et al., Z. Phys. C **69**, 543 (1996)
18. G. Corcella et al., JHEP **01**, 010 (2001)
19. G. Marchesini et al., Comput. Phys. Commun. **67**, 465 (1992)
20. L. Lönnblad, Comput. Phys. Commun. **71**, 15 (1992)
21. M. Skrzypek et al., Comput. Phys. Commun. **119**, 272 (1999) Program KORALW V1.42
22. M. Skrzypek et al., Comput. Phys. Commun. **94**, 216 (1996)
23. M. Skrzypek et al., Phys. Lett. B **372**, 289 (1996)
24. S. Jadach, B.F. L Ward, Z. Was, Phys. Lett. B **449**, 97 (1999)
25. S. Jadach, B.F. L Ward, Z. Was, Comput. Phys. Commun. **130**, 260 (2000)
26. S. Jadach, W. Placzek, B.F.L. Ward, Phys. Lett. B **390**, 298 (1997)
27. T. Sjöstrand, Comput. Phys. Commun. **135**, 238 (2001)
28. R. Engel, J. Ranft, Phys. Rev. D **54**, 4244 (1996)
29. R. Engel, Z. Phys. C **66**, 203 (1995)
30. F.A. Berends, P.H. Daverveldt, R. Kleiss, Nucl. Phys. B **253**, 421 (1985)
31. F.A. Berends, P.H. Daverveldt, R. Kleiss, Comput. Phys. Commun. **40**, 271 (1986)
32. J.A.M. Vermaseren, Nucl. Phys. B **229**, 347 (1983)
33. S. Jadach et al., Comput. Phys. Commun. **140**, 432 (2001) Program YFSWW3 version 1.16
34. S. Jadach et al., Phys. Lett. B **417**, 326 (1998)
35. A. Denner, S. Dittmaier, M. Roth, D. Wackerroth, Nucl. Phys. B **560**, 33 (1999) Program RacoonWW
36. A. Denner, S. Dittmaier, M. Roth, D. Wackerroth, Nucl. Phys. B **587**, 67 (2000)
37. M. Grunewald et al., Four-Fermion Production in Electron-Positron Collisions, CERN 2000-009-A, hep-ph/0005309
38. OPAL Collaboration, G. Abbiendi et al., Eur. Phys. J. C **32**, 453 (2004)
39. OPAL Collaboration, R. Akers et al., Z. Phys. C **63**, 197 (1994)
40. M. Arignon et al., Nucl. Instrum. Methods A **313**, 103 (1992)

41. OPAL Collaboration, G. Abbiendi et al., Phys. Lett. B **580**, 17 (2004)
42. OPAL Collaboration, G. Abbiendi et al., Eur. Phys. J. C **45**, 307 (2006)
43. OPAL Collaboration, G. Alexander et al., Z. Phys. C **52**, 175 (1991)
44. N. Brown, W.J. Stirling, Phys. Lett. B **252**, 657 (1990)
45. S. Bethke, Z. Kunszt, D. Soper, W.J. Stirling, Nucl. Phys. B **370**, 310 (1992)
46. S. Catani et al., Phys. Lett. B **269**, 432 (1991)
47. N. Brown, W.J. Stirling, Z. Phys. C **53**, 629 (1992)
48. OPAL Collaboration, M.Z. Akrawy et al., Phys. Lett. B **253**, 511 (1990)
49. S. Catani, M.H. Seymour, Phys. Lett. B **378**, 287 (1996)
50. R.K. Ellis, D.A. Ross, A.E. Terrano, Nucl. Phys. B **178**, 421 (1981)
51. F.A. Berends, R. Pittau, R. Kleiss, Comput. Phys. Commun. **85**, 437 (1995)
52. D. Karlen, Comput. Phys. **12**, 380 (1998)
53. OPAL Collaboration, P.D. Acton et al., Z. Phys. C **58**, 387 (1993)
54. J. Fujimoto et al., Comput. Phys. Commun. **100**, 128 (1997)
55. T. Sjöstrand, V.A. Khoze, Z. Phys. C **62**, 281 (1994)
56. T. Sjöstrand, V.A. Khoze, Phys. Rev. Lett. **72**, 28 (1994)
57. L. Lönnblad, Z. Phys. C **70**, 107 (1996)
58. L. Lönnblad, T. Sjöstrand, Eur. Phys. J. C **2**, 165 (1998)
59. Equation 32.12 of [60]
60. W.-M. Yao et al., J. Phys. G **33**, 1 (2006)
61. OPAL Collaboration, G. Abbiendi et al., Eur. Phys. J. C **19**, 587 (2001)
62. OPAL Collaboration, G. Abbiendi et al., Eur. Phys. J. C **33**, 463 (2004)
63. ALEPH Collaboration, A. Heister, et al., Eur. Phys. J. C **38**, 147 (2004)
64. DELPHI Collaboration, J. Abdallah, et al., Eur. Phys. J. C **34**, 127 (2004)
65. L3 Collaboration, P. Achard, et al., Phys. Lett. B **600**, 22 (2004)